POSITION AND ORIENTATION CONTROL OF A 6-DOF ROBOT USING FEEDFORWARD ANFIS-PID CONTROLLER

A Thesis Submitted to EIT-M, School of Mechanical and Industrial Engineering in Partial Fulfillment of The Requirements for The Award of The Degree of Master of Science

in

Mechatronics Engineering

by

Gebrekiros Haile

Eitm/Pr134946/10

Under the supervision of

Dr. Betteley Teka

and

Co advisor

Mr. Desta Syoum

MEKELLE UNIVERSITY

ETHIOPIAN INSTITUTE OF TECHNOLOGY-MEKELLE

SCHOOL OF MECHANICAL AND INDUSTRIAL ENGINEERING

December, 2024

DECLARATION

CANDIDATE'S DECLARATION

I hereby declare that this thesis entitled by "POSITION AND ORIENTATION CONTROL OF A 6-DOF ROBOT USING FEEDFORWARD ANFIS-PID CONTROLLER" is the result of my own investigations, except where otherwise stated. I also declare that I have adhered to all principles of academic honesty and integrity and have not misrepresented or fabricated or falsified any idea/data/fact/source in my submission. I understand that any violation of the above will be cause for disciplinary action by the Institute and can also evoke penal action from the sources which have thus not been properly cited or from who, proper permission has not been taken when needed.

Name of Candidate: Gebrekiros Haile

Signature:..... Date:.....

ADVISOR'S DECLARATION

This is to certify that the above declaration made by the candidate is correct to the best of my knowledge and the thesis is adequate for the award of the degree of Master of Science in Mechatronics Engineering.

Advisor: Dr. Betteley Teka

Signature:..... Date:.....

Co-Advisor: Mr. Desta Syoum (MSc.)

Signature:..... Date:.....

THESIS ACCEPTANCE APPROVAL FORM

This is to certify that Mr. Gebrekiros Haile has incorporated all comments forwarded by the external and internal examiners as well as by chairperson during the thesis defense held on.....2024.

Members of the Examination Board

Dr. BETTELEY TEKA	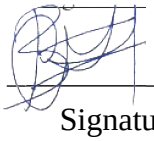	02/04/2025
Supervisor	Signature	Date
Mr. DESTA SYOUM		
Co-Supervisor	Signature	Date
Dr.Zenachew Muluneh	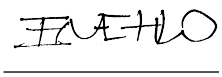	03/04/2025
Internal Examiner	Signature	Date
Dr. Riessom W/goirgis	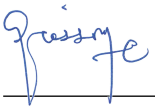	03/04/2025
External Examiner	Signature	Date
Nebyat G/gziabhier	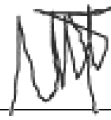	03/04/2025
Chairman	Signature	Date

Confirmation: Industrial Automation and Control Chair

Mr. NEBYAT GEBREGZIABHIER	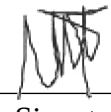	03/04/2025
Chair Head	Signature	Date

ACKNOWLEDGEMENTS

First and foremost, I would like to thank the almighty God for supporting me in each step of my life, and for giving me the ability and privilege to be at the point where I am now. I would like to extend my deepest gratitude to my supervisor Dr. Beteley Teka and my co-supervisor Mr. Desta Syoum (MSc.) for their valuable guidance, advice and motivation they gave me throughout this thesis and throughout my MSc. Study. I would like to thank Mekelle University, Ethiopian Institute of Technology-Mekelle, School of Mechanical and Industrial Engineering, Industrial Automation and Control Chair for the opportunity they gave me to attend this MSc. Program and for their follow up. I would like to thank all my friends and colleagues for their precious friendship, support and ideas. Mostly I would like to thank my family, without their support, I would have never reached to where I am now.

Thank you,

ABSTRACT

Robotic systems with six degrees of freedom (6-DOF) have become essential in high-precision tasks such as industrial welding and surgical operations. These systems necessitate sophisticated control strategies to address the complexities of nonlinear dynamics, actuator behaviors, and external disturbances. In this research, a feedforward Adaptive Neuro-Fuzzy Inference System (ANFIS)-PID controller was developed for the precise position and orientation control of a 6-DOF robotic manipulator. The kinematic model of the robot was formulated using the Denavit-Hartenberg (DH) convention, allowing for the derivation of forward and inverse kinematics. The accuracy of the kinematic model was verified through simulations conducted in MATLAB. A dynamic model, which integrated actuator dynamics for all six joints, was developed using MSC Adams and validated in a co-simulation environment. This high-fidelity model enabled the realistic simulation of the robot's mechanical and dynamic behavior. The ANFIS-PID controller was designed and tested within a MATLAB/Simulink co-simulation environment, which interfaced seamlessly with the dynamic model from MSC Adams. The performance of the developed controller was evaluated in terms of trajectory tracking and disturbance rejection. Results indicated that the controller significantly outperformed traditional PID controllers, achieving position errors below 0.3° under normal and disturbed conditions. These findings highlighted the ANFIS-PID controller's adaptability to nonlinear dynamics and superior performance in comparison to its conventional counterparts. Despite its successes, limitations were identified. Factors such as link elasticity and joint friction were not incorporated into the dynamic model, and the training of the ANFIS model was constrained by computational resources. These omissions have been recommended for future research to enhance the model's accuracy and real-world applicability. Nevertheless, the objectives of this research were achieved, and the potential of hybrid controllers in addressing the challenges of robotic control systems was demonstrated.

Keywords: 6-DOF robot, kinematic modeling, dynamic modeling, ANFIS-PID controller.

TABLE OF CONTENTS

ACKNOWLEDGEMENTS ..... **IV**

ABSTRACT ..... **V**

LIST OF TABLES ..... **VIII**

LIST OF FIGURES ..... **VIII**

LIST OF SYMBOLS ..... **IX**

1. INTRODUCTION **11**

1.1. BACKGROUND 11

1.2. PROBLEM STATEMENT 13

1.3. OBJECTIVES 13

1.3.1. General Objective 13

1.3.2. Specific Objective 14

1.4. METHODOLOGY: AN OVERVIEW 14

1.5. SCOPE AND LIMITATION OF THE RESEARCH 16

1.6. THESIS OUTLINE 17

2. LITERATURE REVIEW **18**

2.1. INTRODUCTION 18

2.2. KINEMATIC AND DYNAMIC MODELING TECHNIQUES 18

2.3. STATE-OF-THE-ART AND CHALLENGES: DYNAMIC MODELING AND CONTROL OF MANIPULATORS 19

3. METHODOLOGY **22**

3.1. INTRODUCTION 22

3.2. KINEMATIC MODELING 24

3.2.1. Forward Kinematics 25

3.2.2. Inverse Kinematics 35

3.3. SAMPLE TRAJECTORY DESIGN 42

3.4. DYNAMIC MODELING OF THE 6 DOF ROBOT 45

3.5. CONTROLLER DESIGN 46

3.5.1. Design of ANFIS-PID controller for position and orientation control 47
3.5.2. Architecture of the ANFIS controller 48
3.5.3. Training and Testing of the ANFIS 52

4. RESULT AND DISCUSSION 56

4.1. VALIDATION OF THE DEVELOPED INFERENCE SYSTEM (ANFIS) 56
4.2. TIME RESPONSE ANALYSIS RESULTS OF THE SYSTEM UNDER NO DISTURBANCE 57
4.3. TIME RESPONSE ANALYSIS RESULTS OF THE ROBOT UNDER DISTURBANCE 60

5. CONCLUSION AND RECOMMENDATION 62

5.1. CONCLUSION 62
5.2. RECOMMENDATION 62

6. REFERENCES 64

7. APPENDICES 70

APPENDIX 1: SOME IMPORTANT TRIGONOMETRIC IDENTITIES 70
APPENDIX-2: 71

LIST OF TABLES

Table 3.1: DH table of the Robot with its range of movements 27
Table 3.2: ANFIS Training Parameters 53

LIST OF FIGURES

Figure 1.1: Common applications of 6 DOF robots [1] 11
Figure 1.2: Denavit–Hartenberg kinematic parameters [12] 14
Figure 1.3: Software configuration used for the design, modeling and simulation of system 15
Figure 3.1: ABB IRB 2600 Versatile Robot 22
Figure 3.2: Methodology followed to achieve the thesis objective 23
Figure 3.3: Role of forward and inverse kinematics 24
Figure 3.4: Denavit–Hartenberg kinematic parameters [12] 25
Figure 3.5: Frame assignment of the robot using right hand rule 26
Figure 3.6: MATLAB Verification of the kinematic chain and the DH table 27
Figure 3.7: $z\, y' x''$ Euler rotation angles 34
Figure 3.8: Forward kinematics Simulink model function block 35
Figure 3.9: Kinematic decoupling of the 6 DOF robot 36
Figure 3.10: Section one Decoupled for position 37
Figure 3.11: Kinematic chain of the first section 39
Figure 3.12: The second segment of the decoupled robot 40
Figure 3.13: Workspace of the Robot 42
Figure 3.14: 3D Trajectory with end effector orientation 43
Figure 3.15: Actuator model included inverse dynamic model of the robot 45
Figure 3.16: ANFIS-PID controller Architecture of ABB robot 48
Figure 3.17: ANFIS controller Architecture 48
Figure 3.18: Segeno fuzzy inference system 49
Figure 3.19 : Input Membership function of the ANFIS 50
Figure 3.20 : Defuzzification of the Sugeno fuzzy Inference system of the ANFIS 51
Figure 3.21: Structure of the 10x10 MF FIS 52
Figure 3.22: Set of PID controllers developed in order to train the ANFIS 53

Figure 3.23: Training error of the ANFIS models 54
Figure 3.24: Fuzzy inference system of the ANFIS of each of the joints..... 55
Figure 4.1: Test results of the six ANFIS models for the training data respectively..... 56
Figure 4.2: Time response of joint1 to joint 4 under no disturbance..... 57
Figure 4.3: Time response of joint 5 and joint 6 under no disturbance 58
Figure 4.4: Time response of the ABB robot for the given trajectory..... 59
Figure 4.5: Response of the ABB robot controllers subjected to a disturbance 60

LIST OF SYMBOLS

a	kinematic link length, kinematic distance between z and ω
a	acceleration vector
$a_i, \alpha_i, d_i, \theta_i$	DH parameters of link (i)
ANFIS	Adaptive Neuro Fuzzy Inference system
API	Application programing interface
B	body coordinate frame
c	Cos
$C(q, \dot{q})$	damping-type matrix of equation of motion
d	joint distance, differential, prismatic joint variable
d_x, d_y, d_z	elements of d
d_i	position vector of the origin of B_i
D	displacement transformation matrix
DH	Denavit-Hartenberg
DOF	degree of freedom
e	error, exponential function
(i)	link number i
q	Joint variables

q_d	desired path of joint
r_i	the element i of r
r_{ij}	the element of row i and column j of a matrix
R	rotation transformation matrix
s	Sin
t	Time
T	homogeneous transformation matrix, tool frame
x, y, z	local coordinate axes
X, Y, Z	global coordinate axes
α	link twist, roll angle of HR frame, angle from z to w about n
θ	Joint angle
θ_{ijk}	$\theta_i + \theta_j + \theta_k$
τ	torque of an actuator
$[\,]^{-1}$	inverse of the matrix [ ]
$[\,]^{T}$	transpose of the matrix [ ]

CHAPTER 1
INTRODUCTION

1.1. Background

Robotic systems, encompassing a broad range of technologies, have revolutionized various industrial and medical applications with their capacity for precise and complex task execution, Figure 1.1. Among these systems, manipulator robots, particularly those with 6 Degrees of Freedom (6-DOF), stand out for their flexibility and capability to perform intricate operations with high accuracy [1][2][3]. These robots are employed in diverse fields, including surgical procedures and welding operations, where meticulous control over both position and orientation is essential for achieving successful outcomes. The 6-DOF robot provides six independent motions typically three translational and three rotational enabling it to reach a vast range of positions and orientations in three-dimensional space. This capability makes 6-DOF robots highly suitable for tasks that require a combination of movement and orientation adjustments[4].

Figure 1.1: Common applications of 6 DOF robots [1]

The use of 6-degree-of-freedom (6-DOF) robots in both surgical and welding applications offers significant advantages due to their ability to perform precise and complex movements in three-dimensional space. In surgical robotics, this capability is crucial for enhancing the accuracy and

control during delicate procedures, allowing surgeons to operate with a level of precision that surpasses traditional manual techniques [5]. This precision is particularly beneficial in minimally invasive surgeries, where the 6-DOF robots can maneuver surgical instruments with exceptional accuracy, leading to improved patient outcomes and reduced recovery times. Similarly, in the welding industry, 6-DOF robots play a critical role in executing welding tasks that demand exact positioning and orientation of the welding torch [6]. The quality of the welds is highly dependent on the robot's ability to maintain consistent positioning and alignment, which ensures the production of strong, defect-free welds. The dynamic nature of welding environments, characterized by factors such as heat, vibration, and material variations, highlights the necessity for robust control systems that can adapt to these challenges while maintaining high performance [7].

The criticality of accuracy and robustness in various robotic applications cannot be overstated, especially in applications like surgical procedures and welding, where precision is paramount. In surgical robotics, even minor deviations in the positioning of instruments can have significant consequences for patient safety and surgical outcomes [8]. Similarly, in welding, inaccuracies can lead to defects in the welds, affecting the structural integrity of the welded components [9]. Therefore, achieving precise control and maintaining robustness in the face of disturbances are essential for ensuring the success of these applications. Traditional control methods, such as Proportional-Integral-Derivative (PID) controllers, have been widely used in various industrial and robotics applications due to their simplicity and ease of implementation. While PID controllers are effective in many scenarios, they often fall short in addressing the complex dynamics and nonlinearities inherent in 6-DOF robotic systems.

One of the primary limitations of classical control methods is their inability to handle the dynamic behavior of actuators accurately. Actuators, which are responsible for driving the robot's joints and links, introduce additional dynamics that can significantly impact the system's performance. Traditional control models often overlook these actuator dynamics, resulting in discrepancies between the modeled and actual system behavior [10]. This oversight can lead to reduced accuracy, stability, and robustness, ultimately affecting the quality and effectiveness of the robotic system's operations.

Classical control methods, including PID controllers, are designed with certain assumptions that may not hold true in complex robotic systems. For instance, these methods typically assume linear system behavior and neglect the impact of nonlinearities and uncertainties. In the context of 6-DOF robots, these assumptions can lead to inadequate control performance, as the robots' dynamics are often nonlinear and coupled. Additionally, classical controllers may struggle to maintain performance in the presence of external disturbances, such as vibrations or changes in the operating environment [11].

1.2. Statement of the problem

The development of a robust position and orientation controller for a 6-degree-of-freedom (6-DOF) welding robot is a critical challenge in robotics, particularly in high-precision applications such as surgical procedures and welding tasks. Traditional control methods, such as PID controllers, often fail to provide the necessary accuracy and disturbance rejection required in these highly dynamic and coupled systems. The challenge is exacerbated by the complex interactions between the robot's multiple degrees of freedom, external disturbances, and the inherent nonlinearities of the system. Moreover, a common issue in modeling such robotic systems is the neglect of actuator dynamics, leading to inaccuracies in the control model and suboptimal performance. Actuators, which drive the robot's movements, have their own dynamics that significantly impact the robot's behavior, especially in fast and precise operations. Ignoring these dynamics can result in controllers that are unable to achieve the desired precision and robustness in real-world scenarios.

To address this problem, a feedforward adaptive neuro fuzzy inference system (ANFIS)-PID controller is proposed, supported by a high-fidelity model of the robot that incorporates actuator dynamics.

1.3. Objectives

1.3.1. General Objective

The objective of this research is to design a feedforward ANFIS-PID controller for precise position and orientation control of a 6-DOF welding robot that, incorporating actuator dynamics to enhance accuracy and robustness.

1.3.2. Specific Objective

The specific Objectives of this research work are:

- To model the kinematic and dynamic model of the 6-DOF welding robot, incorporating actuator dynamics.
- To design a feedforward ANFIS-PID controller tailored for the position and orientation control of a 6-DOF welding robot.
- To evaluate the feedforward ANFIS-PID controller's performance against traditional PID controllers.

1.4. Methodology: An overview

To achieve the objectives of this research, a series of scientific methods and methodologies were followed. The process began with the development of the kinematic model for the 6-DOF welding robot using the Denavit-Hartenberg (DH) convention and the right-hand rule for frame assignment, Figure 1.2, to formulate the forward kinematics. Subsequently, the inverse kinematics solution was derived analytically through geometric methods to provide precise control of the robot's end-effector.

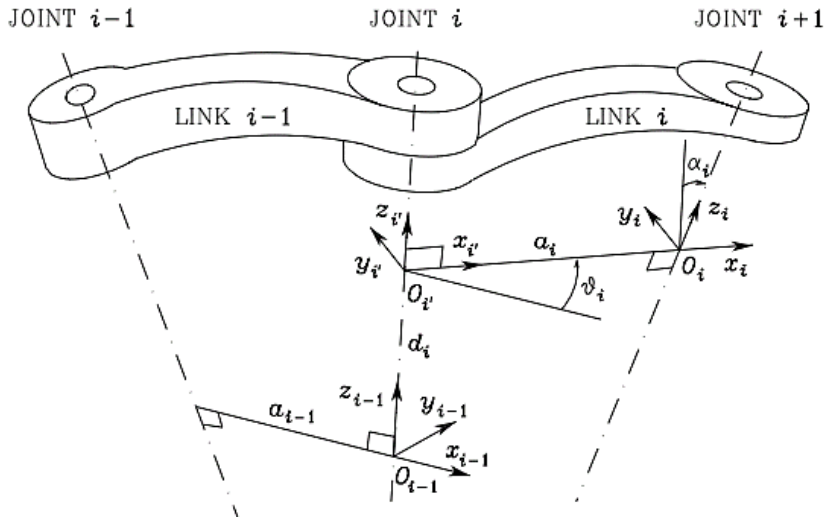

Figure 1.2: Denavit–Hartenberg kinematic parameters [12]

Both the forward and inverse kinematics models were rigorously verified using MATLAB, ensuring their accuracy and functionality in simulating the robot's movements [2][12][13].

Following the kinematic modeling, a high-fidelity dynamic model of the 6-DOF welding robot was developed by integrating SolidWorks with MSC Adams [14]. This approach allowed for detailed modeling of the robot's physical components and their interactions. Additionally, the dynamic model incorporated the actuator dynamics of the servo motors driving the six joints, enhancing the accuracy of the simulations. By integrating these actuator dynamics within MSC Adams, the model provided a comprehensive representation of the robot's behavior under realistic operating conditions, facilitating more precise control and performance assessment.

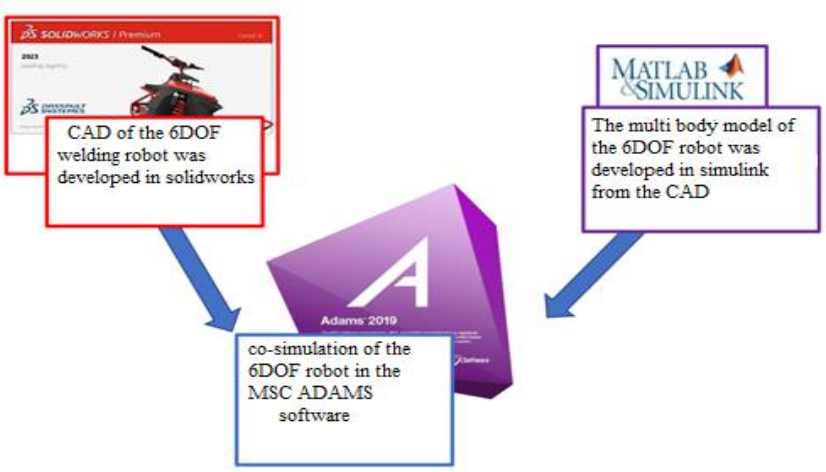

Figure 1.3: Software configuration used for the design, modeling and simulation of system

Subsequently, an ANFIS-PID controller was designed, with its model developed in MATLAB/Simulink co-simulation with MSC Adams, where MSC Adams provided the virtual environment and the high-fidelity dynamic model of the robot [15]. In contrast, MATLAB/Simulink was used for developing the control algorithms and trajectory computations. This integrated approach enabled seamless interaction between the control system and the dynamic model, allowing for comprehensive evaluation of the controller's performance in a simulated environment that accurately reflected the robot's real-world behavior.

Finally, the performance of the ANFIS-PID controller was evaluated through co-simulation, combining the capabilities of MATLAB/Simulink and MSC Adams. The co-simulation focused on position and orientation control of the 6-DOF welding robot, where MATLAB/Simulink implemented the control algorithms and trajectory computations, while MSC Adams provided the virtual environment and dynamic model of the robot. This integrated approach enabled a comprehensive evaluation of the ANFIS-PID controller's effectiveness in achieving precise positioning and orientation, as well as a comparison with traditional control methods, such as standalone PID controllers. The results were analyzed to highlight the advantages of the ANFIS-PID controller in terms of accuracy, adaptability to non-linear dynamics, disturbance rejection, and overall system performance.

1.5. Scope and Limitation of the Research

The research primarily focused on the development and implementation of a feedforward ANFIS-PID controller for the position and orientation control of a 6-degree-of-freedom (6-DOF) welding robot. Despite the comprehensive approach, the research is subject to several limitations. The kinematic and dynamic models are built on assumptions such as rigid body dynamics and ideal joint actuations, which may not fully capture real-world complexities like flexibility in the robot's links or joint friction. The research is predominantly simulation-based, and the findings from the co-simulation environment may differ from real-world hardware implementations due to factors like sensor noise and unmodeled dynamics that are not fully addressed in simulations. Additionally, the high fidelity of the dynamic model, while offering detailed insights, increases computational complexity, potentially limiting the real-time applicability of the controller in scenarios requiring rapid response. Finally, the reliance on a virtual environment for validation means that certain practical challenges, such as mechanical wear and tear, thermal effects, and unexpected disturbances, are not tested within this research, pointing to areas where further investigation and practical trials are necessary to fully realize the controller's potential.

1.6. Thesis Outline

This thesis is organized into five chapters. Chapter 1 introduces the research background, problem statement, objectives, and methodology, highlighting the challenges in precise position and orientation control of 6-DOF robotic manipulators. Chapter 2 reviews relevant literature, focusing on kinematic and dynamic modeling techniques, current control strategies, and the gaps in addressing nonlinearities and actuator dynamics. Chapter 3 presents the methodology, detailing the development of kinematic and dynamic models using the Denavit-Hartenberg convention, SolidWorks, and MSC Adams, alongside the design and training of the ANFIS-PID controller in MATLAB/Simulink. Chapter 4 discusses the results and analysis, comparing the performance of the proposed controller with traditional PID controllers and evaluating its trajectory tracking and disturbance rejection capabilities. Finally, Chapter 5 provides conclusions and recommendations, summarizing the achievements, limitations, and potential directions for future research to enhance the control system's real-world applicability.

CHAPTER 2
LITERATURE REVIEW

2.1. Introduction

The field of robotics has seen significant advancements over the past few decades, with 6-degree-of-freedom (6-DOF) robotic systems playing a pivotal role in various high-precision applications, such as surgical procedures and industrial welding. These robots require sophisticated control systems to manage their complex kinematics and dynamics, ensuring precise position and orientation control [16][17]. However, the challenges associated with nonlinearities, actuator dynamics, and external disturbances necessitate the development of robust control strategies [18]. Traditional controllers often struggle to meet the demanding requirements of such systems, particularly in environments where accuracy, robustness, and disturbance rejection are critical [19].

This literature review examined advancements in control strategies for 6-DOF robots, with an emphasis on the role of feedforward ANFIS-PID controllers in addressing these challenges. Additionally, it delves into the kinematic and dynamic modeling techniques used to accurately represent these robots, along with the applications of these systems in the fields of surgery and welding [20][21]. Finally, a critical analysis of existing research highlights the gaps and areas for further exploration in developing high-fidelity models and robust controllers for 6-DOF robotic systems [22].

2.2. Kinematic and Dynamic Modeling Techniques

Accurate kinematic and dynamic modeling is crucial for the effective control of 6-degree-of-freedom (6-DOF) robotic systems. Kinematic modeling involves the description of the robot's motion without considering the forces and torques that cause this motion. The Denavit-Hartenberg (DH) convention is widely used for this purpose, providing a systematic method to represent the robot's joint and link parameters and establish the forward and inverse kinematic relationships [23]. The forward kinematic model computes the position and orientation of the end-effector given the joint angles, while the inverse kinematic model determines the joint angles required to achieve a desired end-effector pose [24]. These models are essential for controlling the robot's movements with high precision and are typically verified through simulation tools such as MATLAB to ensure accuracy and reliability [25].

Dynamic modeling, on the other hand, incorporates the forces and torques that drive the robot's movement, providing a more comprehensive representation of the robot's behavior. High-fidelity dynamic models are developed to capture the complex interactions between the robot's joints and actuators, including factors like friction and inertia[26]. The integration of actuator dynamics is critical, as servo motors and other actuators introduce additional complexities that can affect the robot's performance. Simulation tools such as MSC Adams are employed to develop these dynamic models, allowing for detailed analysis and validation under various operational conditions [27]. The combination of kinematic and dynamic modeling is crucial for designing and testing advanced control strategies, ensuring that the control algorithms account for both the motion and forces involved. The use of co-simulation, where tools like MSC Adams and MATLAB/Simulink are integrated, enhances the modeling process by combining the strengths of each platform. MSC Adams provides a detailed virtual environment for simulating the robot's dynamic behavior, while MATLAB/Simulink offers powerful capabilities for control algorithm development and trajectory planning[28]. This approach allows for a more accurate and comprehensive evaluation of the control strategies in a realistic simulation environment.

2.3. State-of-the-Art and Challenges: Dynamic Modeling and Control of Manipulators

In the realm of robotic control, particularly for 6-degree-of-freedom (6-DOF) systems, considerable attention has been directed toward developing advanced control methods to ensure precision and robustness. Conventional control techniques, such as Proportional-Integral-Derivative (PID) controllers, have remained prevalent due to their straightforward implementation and proven effectiveness in handling linear system dynamics [29], [30]. These controllers are particularly suitable for applications with minimal system complexity and limited non-linear interactions. However, in scenarios involving intricate, non-linear, and coupled dynamics hallmarks of 6-DOF robotic systems the performance of PID controllers is often inadequate. This inadequacy is especially pronounced in applications demanding high accuracy and fast response times, such as industrial welding and surgical robotics, where even slight control errors can significantly affect overall system performance [31], [32], [33]. To address these limitations, advanced control strategies like ANFIS, Fuzzy Logic Control (FLC), and Model Predictive Control (MPC) have been proposed [33], [34], [35], [36], [37], [38].

Among those Feedforward ANFIS-PID controllers have emerged as a promising alternative to conventional PID and standalone ANFIS controllers, offering significant improvements in control performance. These controllers combine the strengths of ANFIS's adaptability and the simplicity of PID control, resulting in a hybrid approach capable of addressing the limitations inherent in each method. Compared to traditional PID controllers, feedforward ANFIS-PID systems provide superior handling of non-linear and time-varying dynamics, enabling more accurate tracking of complex trajectories and rejection of disturbances in real-time applications [39], [40], [41].

The integration of a feedforward mechanism further enhances performance by compensating for predictable disturbances and improving the system's response time, particularly in applications with rapidly changing dynamics. This proactive compensation reduces overshoot and settling time, achieving smoother and more precise control compared to PID controllers alone [40]. Additionally, ANFIS-PID controllers surpass standalone ANFIS systems by leveraging the PID component for improved stability and robustness, particularly in scenarios involving high-frequency disturbances or model inaccuracies[42], [43]. Moreover, feedforward ANFIS-PID controllers exhibit enhanced computational efficiency when compared to advanced control methods such as MPC. Their hybrid nature reduces the design complexity, making them more feasible for real-time applications and systems with limited computational resources [42], [44]. These attributes position feedforward ANFIS-PID controllers as a robust and efficient solution for addressing the challenges associated with controlling dynamic, non-linear systems, particularly in robotics and other high-performance applications.

Despite the advancements in control strategies, there are notable gaps in the literature, particularly concerning the control of 6-DOF robots [45]. Many existing studies focus on the theoretical development of advanced control algorithms but often do not incorporate comprehensive models that accurately reflect the dynamics of the robotic system, including the actuator dynamics [3], [16],[46]. Actuator dynamics, which include the effects of inertia, friction, backlash, and non-linearities of servo motors, play a critical role in the precise control of robotic joints [47], [48],[49]. Neglecting these dynamics in the modeling phase can lead to discrepancies between the simulated control performance and real-world outcomes [50], [51]. This oversight is particularly problematic in applications like surgical robotics, where precision and reliability are paramount, and in

welding, where the quality of the final product is highly dependent on the accuracy of the robot's movements.

The implications of these gaps are significant for the development of high-fidelity models and controllers. Without an accurate model that includes all relevant dynamics, even the most sophisticated control algorithms may fail to deliver the desired level of performance in practical applications. High-fidelity modeling, which incorporates detailed representations of both the robot's mechanical structure and its actuator dynamics, is essential for developing effective control strategies. These models enable more accurate simulations, allowing for the rigorous testing and validation of control algorithms under realistic conditions [2], [16], [52]. This approach ensures that the controllers can handle the complexities of real-world operations, such as non-linearities, disturbances, and variations in load conditions. For instance, in surgical robotics, the ability to accurately model and control the robot's movements can lead to safer and more effective surgeries. In the welding industry, such advancements can result in higher quality welds, reduced defects, and increased production efficiency. Therefore, addressing the existing gaps in the literature through comprehensive modeling and the application of advanced control techniques is essential for the continued evolution of 6-DOF robotic systems.

2.4 Summery of literature review

The literature review highlights the advancements in 6-DOF robotic control, emphasizing the role of feedforward ANFIS-PID controllers in improving precision, robustness, and disturbance rejection. Traditional PID controllers are effective for simple linear systems but struggle with nonlinearities and actuator dynamics, which are crucial in applications like welding and surgical robotics. Advanced control strategies, such as ANFIS, Fuzzy Logic, and MPC, have been proposed, but they come with computational complexities or lack real-time feasibility.

Despite these advancements, a critical gap exists in the accurate modeling of actuator dynamics in 6-DOF robotic control. Many existing studies focus on control algorithms without fully incorporating actuator dynamics, including inertia, friction, backlash, and nonlinearities of servo motors. This omission can lead to a mismatch between simulated and real-world performance, limiting the controller’s effectiveness in high-precision applications.

CHAPTER 3

METHODOLOGY

3.1. Introduction

This chapter focuses on the development and simulation of the kinematic and dynamic models, as well as the design of the controller for the ABB IRB 2600, a 6-degree-of-freedom (6-DOF) industrial robot. The ABB IRB 2600 has been selected for this research due to its widespread application in various high-precision and demanding tasks, particularly in surgical robotics and industrial manufacturing sectors, including welding [53]. The robot's versatility, coupled with its advanced motion capabilities, makes it an ideal subject for developing and testing sophisticated control algorithms [54]. Understanding the kinematics and dynamics of this robot is essential for accurate simulation and control, ensuring that it meets the rigorous demands of these applications. This chapter details the process of deriving the mathematical models necessary for effective control design and implementation.

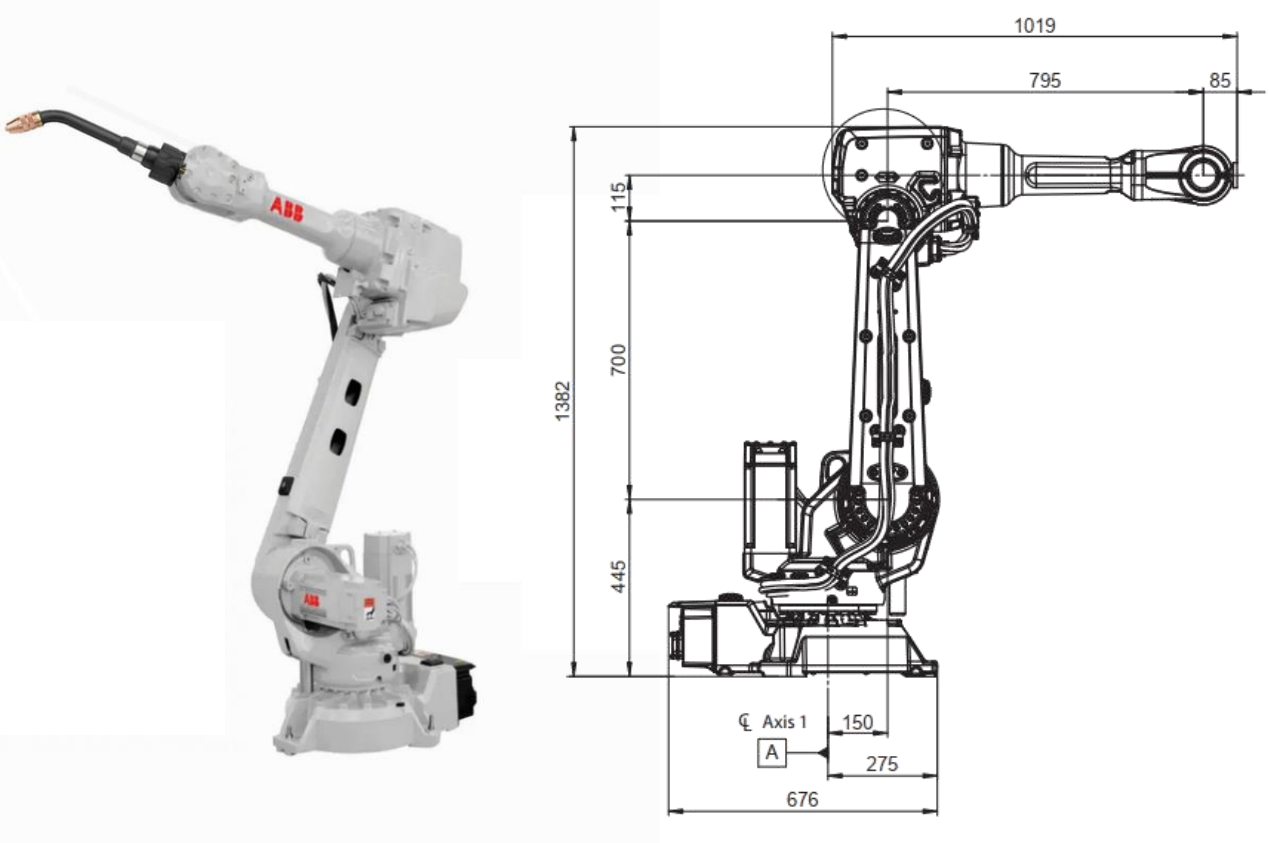

Figure 3.1: ABB IRB 2600 Versatile Robot

To achieve accurate modeling, a series of established methodologies were employed. The Denavit-Hartenberg (DH) convention was utilized to develop the forward kinematic model, while the inverse kinematics was derived analytically using geometric methods. These models were subsequently verified using MATLAB to ensure their accuracy.

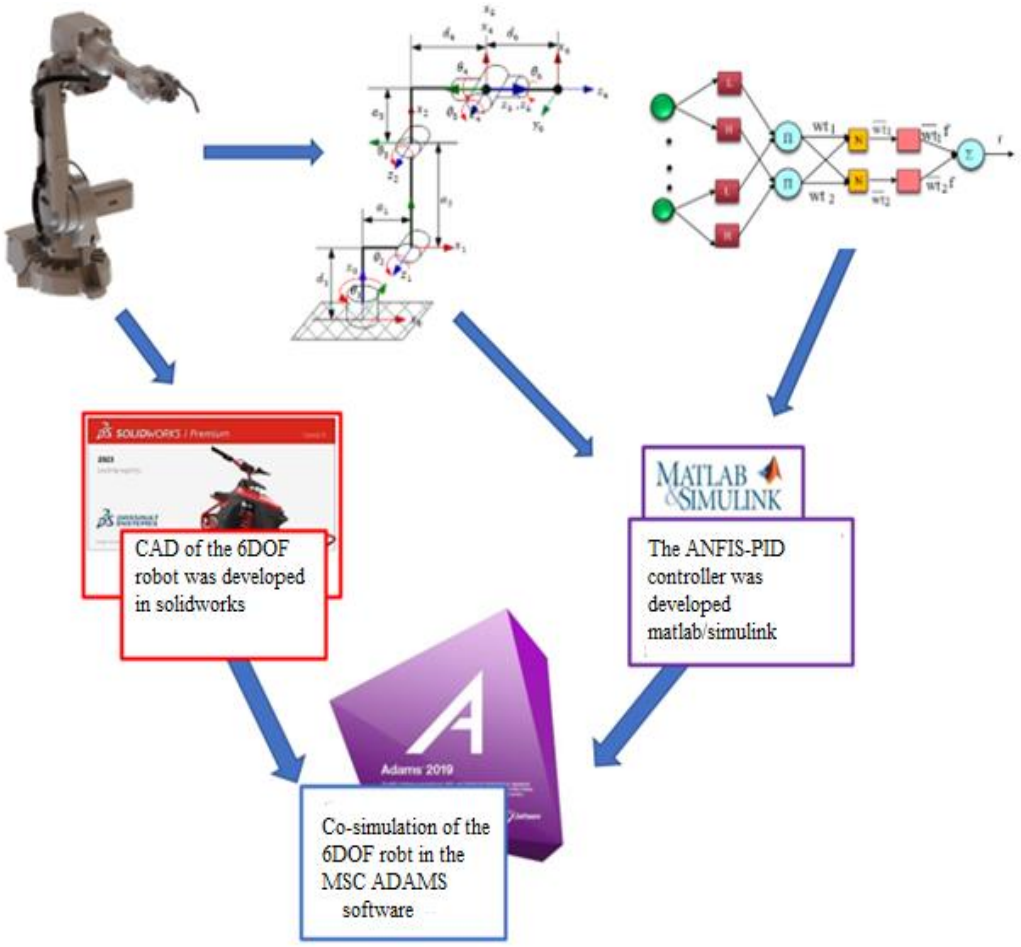

For the dynamic modeling, a high-fidelity model was constructed by integrating SolidWorks and MSC Adams with MATLAB/Simulink, incorporating the actuator dynamics of the servo motors for all six joints, Figure 3.2. Following the kinematic and dynamic modeling, the controller design was developed with the objective of ensuring precise and smooth movements of the robot's joints, thereby allowing accurate execution of tasks. This chapter elaborates on the methodologies applied

across each phase of the modeling and design processes, offering a detailed account of the systematic approach undertaken to achieve the desired robotic functionalities.

3.2. Kinematic Modeling

Kinematic modeling is a cornerstone of robotic systems analysis, serving as the foundation for understanding and controlling the movement of robots. It involves the study of motion without considering the forces that cause it, focusing primarily on the relationships between the various parts of a robot as they move [2],[52]. In essence, kinematic modeling allows to predict the position and orientation of a robot's end-effector based on the configurations of its joints and links. For robotic manipulators, kinematic modeling is divided into two main components: forward kinematics and inverse kinematics. Forward kinematics deals with determining the end-effector's position and orientation given the joint parameters, such as angles or displacements, Figure 3.3. This process is vital for tasks where the exact position of the end-effector needs to be known for each possible configuration of the robot's joints.

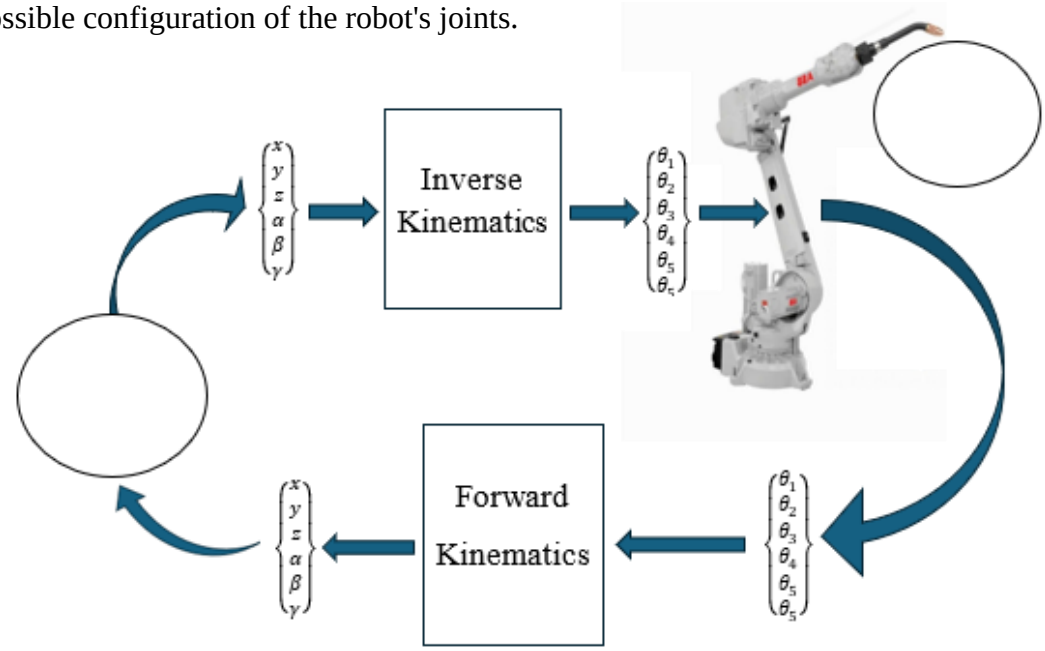

Figure 3.3: Role of forward and inverse kinematics

Inverse kinematics, on the other hand, involves calculating the necessary joint parameters to achieve a desired position and orientation of the end-effector. This is particularly important for path planning and task execution, where specific positions need to be reached by the robot [1],[4].

Kinematic modeling is not only critical for the design and simulation of robots but also for real-time control during operations. In applications such as surgical robotics and industrial automation, the ability to precisely control the robot's movements is essential. Any errors in the kinematic model can lead to inaccuracies in the robot's motion, potentially causing significant issues in tasks that require high precision. Therefore, a robust kinematic model is indispensable for the successful implementation of any robotic system, ensuring that it operates as intended in a variety of environments and conditions.

3.2.1. Forward Kinematics

The forward kinematics of a robotic manipulator involves determining the position and orientation of the robot's end-effector based on the joint parameters [16]. This aspect is fundamental to understanding how the robot's structure influences its ability to reach specific points in space, which is critical for tasks requiring high precision, such as welding and surgical procedures. The importance of forward kinematics extends beyond mere position calculation; it is essential for implementing joint space control architectures [2]. In such architectures, control algorithms operate within the joint space, where each joint's movement is controlled individually but with the understanding that all joints collectively determine the end-effector's final position and orientation

In the context of a 6-DOF robot, such as the ABB IRB 2600, the forward kinematics problem is complex due to the multiple joints and axes of rotation. Each joint contributes to the overall position and orientation of the end-effector, making the calculation of these parameters critical for the robot's operation. The Denavit-Hartenberg (DH) convention is used to address this complexity by providing a systematic method for modeling the kinematic chains [55].

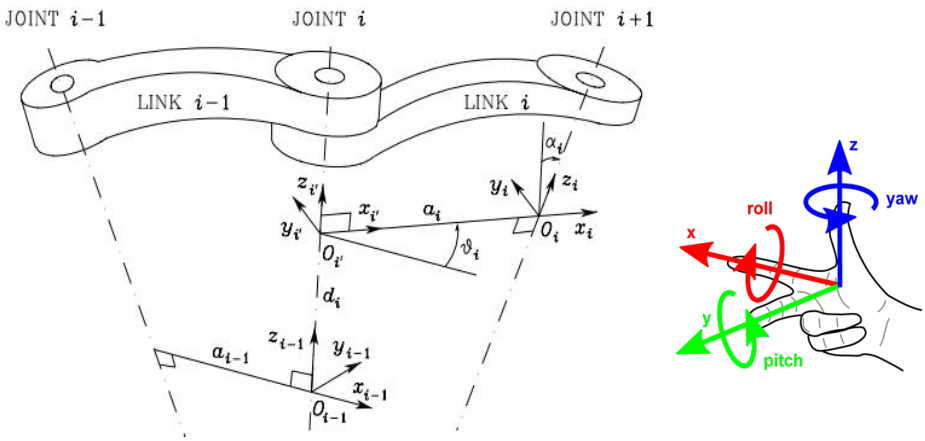

Figure 3.4: Denavit–Hartenberg kinematic parameters [12]

Prior to the development of the homogeneous transformation matrices, the kinematic chain of the robot was carefully developed, and reference frames were assigned to each link according to the DH convention and right-hand rule.

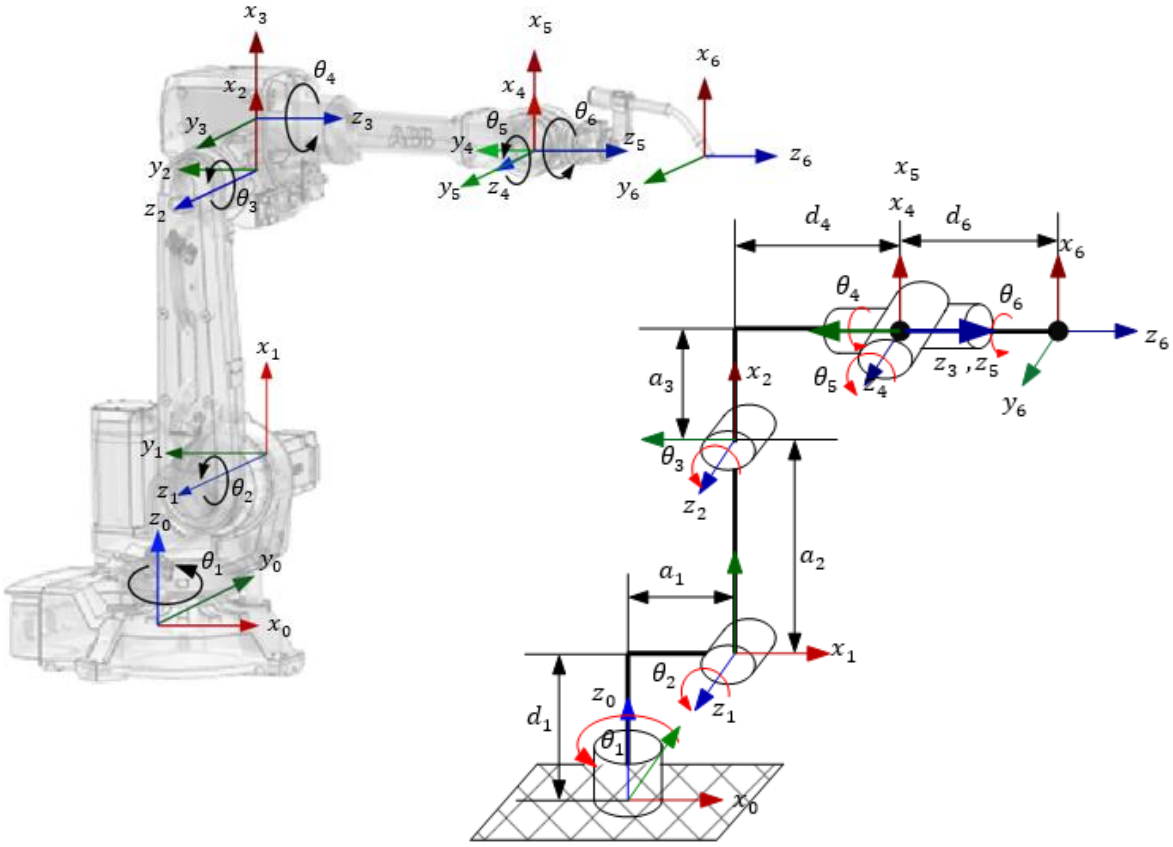

Figure 3.5: Frame assignment of the robot using right hand rule

Following the successful development of the kinematic chain and frame assignment, the DH parameters were parameterized and tabulated, Table 3.1, based on the geometric properties of the ABB robot. These parameters include four key variables: the link length (ai), which is the distance between the z-axes of two consecutive frames along the x-axis; the link twist (αi), representing the angle between the z-axes of two consecutive frames about the x-axis; the link offset (di), which is the distance along the z-axis from one x-axis to the next; the joint angle (θi), denoting the rotation around the z-axis from one x-axis to the next; and the joint offset.

Table 3.1: DH table of the Robot with its range of movements

	a_i	α_i	d_i	θ_i	offset	Range of movements
Joint-1	150	90	445	θ_1	0	$+180^0$ to -180^0
Joint -2	700	0	0	θ_2	90	$+155^0$ to -95^0
Joint -3	115	90	0	θ_3	0	$+75^0$ to -180^0
Joint -4	0	-90	795	θ_4	0	$+175^0$ to -175^0
Joint -5	0	90	0	θ_5	0	$+120^0$ to -120^0
Joint -6	0	0	400	θ_6	0	$+400^0$ to -400^0

Before diving into the forward kinematics computation, the developed DH parameters and the kinematic chain were validated for accuracy using Peter Corke's Robotics and Computer Vision Toolbox[56]. This validation step was crucial to ensure that the mathematical models accurately represent the physical robot, providing a reliable foundation for subsequent kinematic analysis and control algorithm development.

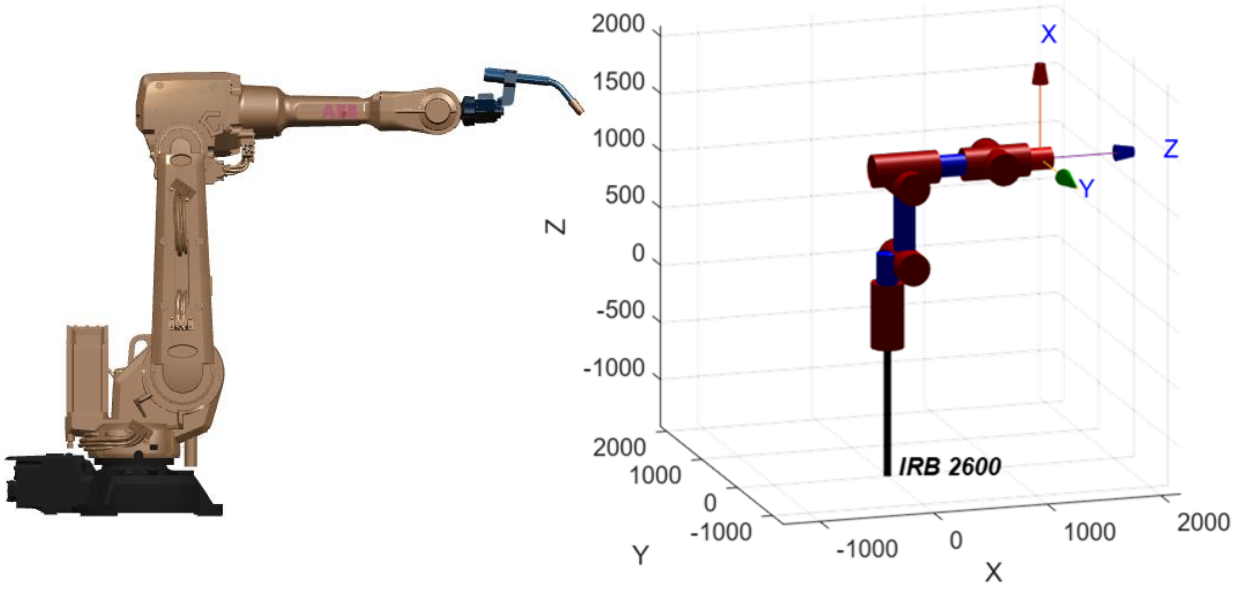

Figure 3.6: MATLAB Verification of the kinematic chain and the DH table

After the validation of the developed kinematic chain and DH parameters, the individual homogeneous transformations from each joint to the next, starting from joint 1 through to joint 6, were computed using the DH homogeneous transformation matrix,(3.1). This step provided a sequential mapping of the robot's joint configurations, allowing for the accurate determination of the position and orientation of the end-effector relative to the base frame.

$$T_i^{i-1} = \begin{bmatrix} cos\theta_i & -sin\theta_i cos\alpha_i & sin\theta_i sin\alpha_i & a_i cos\theta_i \\ sin\theta_i & cos\theta_i cos\alpha_i & -cos\theta_i sin\alpha_i & a_i sin\theta_i \\ 0 & sin\alpha_i & cos\alpha_i & d_i \\ 0 & 0 & 0 & 1 \end{bmatrix} \quad (3.1)$$

By Substituting the respective DH parameters of each of the links of the ABB robot in to equation (3.1), the respective transformation matrices of each joint to their respective frames were found to be:

$$T_1^0 = \begin{bmatrix} \cos(\theta_1) & 0 & \sin(\theta_1) & 150\cos(\theta_1) \\ \sin(\theta_1) & 0 & -\cos(\theta_1) & 150\sin(\theta_1) \\ 0 & 1 & 0 & 445 \\ 0 & 0 & 0 & 1 \end{bmatrix}$$

$$T_2^1 = \begin{bmatrix} \cos\left(\theta_2+\frac{\pi}{2}\right) & \cos\left(\theta_2+\frac{\pi}{2}\right) & 0 & 700\cos\left(\theta_2+\frac{\pi}{2}\right) \\ \sin\left(\theta_2+\frac{\pi}{2}\right) & \cos\left(\theta_2+\frac{\pi}{2}\right) & 0 & 700\sin\left(\theta_2+\frac{\pi}{2}\right) \\ 0 & 0 & 1 & 0 \\ 0 & 0 & 0 & 1 \end{bmatrix}$$

$$T_3^2 = \begin{bmatrix} \cos(\theta_3) & 0 & \sin(\theta_3) & 115\cos(\theta_3) \\ \sin(\theta_3) & 0 & -\cos(\theta_3) & 115\sin(\theta_3) \\ 0 & 1 & 0 & 0 \\ 0 & 0 & 0 & 1 \end{bmatrix} \quad (3.2)$$

$$T_4^3 = \begin{bmatrix} \cos(\theta_4) & 0 & -\sin(\theta_4) & 0 \\ \sin(\theta_4) & 0 & \cos(\theta_4) & 0 \\ 0 & -1 & 0 & 795 \\ 0 & 0 & 0 & 1 \end{bmatrix}$$

$$T_5^4 = \begin{bmatrix} \cos(\theta_6) & -\sin(\theta_6) & 0 & 0 \\ \sin(\theta_6) & \cos(\theta_6) & 0 & 0 \\ 0 & 0 & 1 & 400 \\ 0 & 0 & 0 & 1 \end{bmatrix}$$

$$T_6^5 = \begin{bmatrix} \cos(\theta_6) & -\sin(\theta_6) & 0 & 0 \\ \sin(\theta_6) & \cos(\theta_6) & 0 & 0 \\ 0 & 0 & 1 & 400 \\ 0 & 0 & 0 & 1 \end{bmatrix}$$

The homogeneous transformation matrix of the end-effector, the tip of the welding torch, relative to the base of the robot, T_6^0, was computed by multiplying the successive individual transformations from the tip of the end-effector to the base frame.

$$T_6^0 = T_1^0 T_2^1 T_3^2 T_4^3 T_5^4 T_6^5 = \begin{bmatrix} n_x & n_y & n_z & P_x \\ o_x & o_y & o_z & P_y \\ a_x & a_y & a_z & P_z \\ 0 & 0 & 0 & 1 \end{bmatrix} \quad (3.3)$$

where:

$$n_x = \cos(\theta_6)\left(\cos(\theta_5)\left(\cos(\theta_4)\left(\cos(\theta_1)\cos(\theta_3)\cos\left(\theta_2+\frac{\pi}{2}\right)-\sin(\theta_3)\cos(\theta_1)\sin\left(\theta_2+\frac{\pi}{2}\right)\right)+\sin(\theta_1)\sin(\theta_4)\right)\right.$$
$$\left.-\ \sin(\theta_5)\left(\sin(\theta_3)\cos(\theta_1)\cos\left(\theta_2+\frac{\pi}{2}\right)+\cos(\theta_1)\cos(\theta_3)\sin\left(\theta_2+\frac{\pi}{2}\right)\right)\right)$$
$$+\sin(\theta_6)\left((-\sin(\theta_4))\left(\cos(\theta_1)\cos(\theta_3)\cos\left(\theta_2+\frac{\pi}{2}\right)-\sin(\theta_3)\cos(\theta_1)\sin\left(\theta_2+\frac{\pi}{2}\right)\right)+\sin(\theta_1)\cos(\theta_4)\right)$$

$$n_y = \cos(\theta_6)\left(\cos(\theta_5)\left(\cos(\theta_4)\left(\sin(\theta_1)\cos(\theta_3)\cos\left(\theta_2+\frac{\pi}{2}\right)-\sin(\theta_1)\sin(\theta_3)\sin\left(\theta_2+\frac{\pi}{2}\right)\right)-\sin(\theta_4)\cos(\theta_1)\right)\right.$$
$$\left.-\ \sin(\theta_5)\left(\sin(\theta_1)\sin(\theta_3)\cos\left(\theta_2+\frac{\pi}{2}\right)+\sin(\theta_1)\cos(\theta_3)\sin\left(\theta_2+\frac{\pi}{2}\right)\right)\right)$$
$$-\sin(\theta_6)\left(\sin(\theta_4)\left(\sin(\theta_1)\cos(\theta_3)\cos\left(\theta_2+\frac{\pi}{2}\right)-\sin(\theta_1)\sin(\theta_3)\sin\left(\theta_2+\frac{\pi}{2}\right)\right)+\cos(\theta_1)\cos(\theta_4)\right)$$

$$n_z = \cos(\theta_6)\left(\cos(\theta_4)\cos(\theta_5)\left(\sin(\theta_3)\cos\left(\theta_2+\frac{\pi}{2}\right)+\cos(\theta_3)\sin\left(\theta_2+\frac{\pi}{2}\right)\right)+\right.$$
$$\left.\sin(\theta_5)\left(\cos(\theta_3)\cos\left(\theta_2+\frac{\pi}{2}\right)-\sin(\theta_3)\sin\left(\theta_2+\frac{\pi}{2}\right)\right)\right)-\sin(\theta_4)\sin(\theta_6)\left(\sin(\theta_3)\cos\left(\theta_2+\frac{\pi}{2}\right)+\cos(\theta_3)\sin\left(\theta_2+\frac{\pi}{2}\right)\right)$$

$$o_x = (-\sin(\theta_6))\left(\cos(\theta_5)\left(\cos(\theta_4)\left(\cos(\theta_1)\cos(\theta_3)\cos\left(\theta_2+\frac{\pi}{2}\right)-\sin(\theta_3)\cos(\theta_1)\sin\left(\theta_2+\frac{\pi}{2}\right)\right)+\sin(\theta_1)\sin(\theta_4)\right)\right.$$
$$\left.-\ \sin(\theta_5)\left(\sin(\theta_3)\cos(\theta_1)\cos\left(\theta_2+\frac{\pi}{2}\right)+\cos(\theta_1)\cos(\theta_3)\sin\left(\theta_2+\frac{\pi}{2}\right)\right)\right)$$
$$+\cos(\theta_6)\left((-\sin(\theta_4))\left(\cos(\theta_1)\cos(\theta_3)\cos\left(\theta_2+\frac{\pi}{2}\right)-\sin(\theta_3)\cos(\theta_1)\sin\left(\theta_2+\frac{\pi}{2}\right)\right)+\sin(\theta_1)\cos(\theta_4)\right)$$

$$o_y = (-\sin(\theta_6))\left(\cos(\theta_5)\left(\cos(\theta_4)\left(\sin(\theta_1)\cos(\theta_3)\cos\left(\theta_2+\frac{\pi}{2}\right)-\sin(\theta_1)\sin(\theta_3)\sin\left(\theta_2+\frac{\pi}{2}\right)\right)-\sin(\theta_4)\cos(\theta_1)\right)\right.$$
$$\left.-\ \sin(\theta_5)\left(\sin(\theta_1)\sin(\theta_3)\cos\left(\theta_2+\frac{\pi}{2}\right)+\sin(\theta_1)\cos(\theta_3)\sin\left(\theta_2+\frac{\pi}{2}\right)\right)\right)$$
$$-\cos(\theta_6)\left(\sin(\theta_4)\left(\sin(\theta_1)\cos(\theta_3)\cos\left(\theta_2+\frac{\pi}{2}\right)-\sin(\theta_1)\sin(\theta_3)\sin\left(\theta_2+\frac{\pi}{2}\right)\right)+\cos(\theta_1)\cos(\theta_4)\right)$$

$$o_z = (-\sin(\theta_6))\left(\cos(\theta_4)\cos(\theta_5)\left(\sin(\theta_3)\cos\left(\theta_2+\frac{\pi}{2}\right)+\cos(\theta_3)\sin\left(\theta_2+\frac{\pi}{2}\right)\right)+\right.$$
$$\left.\sin(\theta_5)\left(\cos(\theta_3)\cos\left(\theta_2+\frac{\pi}{2}\right)-\sin(\theta_3)\sin\left(\theta_2+\frac{\pi}{2}\right)\right)\right)-\sin(\theta_4)\cos(\theta_6)\left(\sin(\theta_3)\cos\left(\theta_2+\frac{\pi}{2}\right)+\cos(\theta_3)\sin\left(\theta_2+\frac{\pi}{2}\right)\right)$$

$$a_x = \sin(\theta_5)\left(\cos(\theta_4)\left(\cos(\theta_1)\cos(\theta_3)\cos\left(\theta_2+\frac{\pi}{2}\right)-\sin(\theta_3)\cos(\theta_1)\sin\left(\theta_2+\frac{\pi}{2}\right)\right) + \sin(\theta_1)\sin(\theta_4)\right) +$$
$$\cos(\theta_5)\left(\sin(\theta_3)\cos(\theta_1)\cos\left(\theta_2+\frac{\pi}{2}\right)+\cos(\theta_1)\cos(\theta_3)\sin\left(\theta_2+\frac{\pi}{2}\right)\right)$$

$$a_y = \sin(\theta_5)\left(\cos(\theta_4)\left(\sin(\theta_1)\cos(\theta_3)\cos\left(\theta_2+\frac{\pi}{2}\right)-\sin(\theta_1)\sin(\theta_3)\sin\left(\theta_2+\frac{\pi}{2}\right)\right) - \sin(\theta_4)\cos(\theta_1)\right) +$$
$$\cos(\theta_5)\left(\sin(\theta_1)\sin(\theta_3)\cos\left(\theta_2+\frac{\pi}{2}\right)+\sin(\theta_1)\cos(\theta_3)\sin\left(\theta_2+\frac{\pi}{2}\right)\right)$$

$$a_z = \sin(\theta_5)\cos(\theta_4)\left(\sin(\theta_3)\cos\left(\theta_2+\frac{\pi}{2}\right) + \cos(\theta_3)\sin\left(\theta_2+\frac{\pi}{2}\right)\right) +$$
$$\cos(\theta_5)\left(\cos(\theta_3)\cos\left(\theta_2+\frac{\pi}{2}\right)-\sin(\theta_3)\sin\left(\theta_2+\frac{\pi}{2}\right)\right)$$

$$P_x = l_6\left(\sin(\theta_5)\left(\cos(\theta_4)\left(\cos(\theta_1)\cos(\theta_3)\cos\left(\theta_2+\frac{\pi}{2}\right)-\sin(\theta_3)\cos(\theta_1)\sin\left(\theta_2+\frac{\pi}{2}\right)\right)+\sin(\theta_1)\sin(\theta_4)\right) +$$
$$\cos(\theta_5)\left(\sin(\theta_3)\cos(\theta_1)\cos\left(\theta_2+\frac{\pi}{2}\right)+\cos(\theta_1)\cos(\theta_3)\sin\left(\theta_2+\frac{\pi}{2}\right)\right)\right) +$$
$$l_5\left(\sin(\theta_3)\cos(\theta_1)\cos\left(\theta_2+\frac{\pi}{2}\right)+\cos(\theta_1)\cos(\theta_3)\sin\left(\theta_2+\frac{\pi}{2}\right)\right) + l_4\cos(\theta_1)\cos(\theta_3)\cos\left(\theta_2+\frac{\pi}{2}\right) -$$
$$l_4\sin(\theta_3)\cos(\theta_1)\sin\left(\theta_2+\frac{\pi}{2}\right) + l_3\cos(\theta_1)\cos\left(\theta_2+\frac{\pi}{2}\right) + l_2\cos(\theta_1)$$

$$P_y = l_6\left(\sin(\theta_5)\left(\cos(\theta_4)\left(\sin(\theta_1)\cos(\theta_3)\cos\left(\theta_2+\frac{\pi}{2}\right)-\sin(\theta_1)\sin(\theta_3)\sin\left(\theta_2+\frac{\pi}{2}\right)\right)-\sin(\theta_4)\cos(\theta_1)\right)+\right.$$
$$\left.\cos(\theta_5)\left(\sin(\theta_1)\sin(\theta_3)\cos\left(\theta_2+\frac{\pi}{2}\right)+\sin(\theta_1)\cos(\theta_3)\sin\left(\theta_2+\frac{\pi}{2}\right)\right)\right)+$$
$$l_5\left(\sin(\theta_1)\sin(\theta_3)\cos\left(\theta_2+\frac{\pi}{2}\right)+\sin(\theta_1)\cos(\theta_3)\sin\left(\theta_2+\frac{\pi}{2}\right)\right)+l_4\sin(\theta_1)\cos(\theta_3)\cos\left(\theta_2+\frac{\pi}{2}\right)-$$
$$l_4\sin(\theta_1)\sin(\theta_3)\sin\left(\theta_2+\frac{\pi}{2}\right)+l_3\sin(\theta_1)\cos\left(\theta_2+\frac{\pi}{2}\right)+l_2\sin(\theta_1)$$

$$P_z = l_6\left(\sin(\theta_5)\cos(\theta_4)\left(\sin(\theta_3)\cos\left(\theta_2+\frac{\pi}{2}\right)+\cos(\theta_3)\sin\left(\theta_2+\frac{\pi}{2}\right)\right)-\right.$$
$$\left.\cos(\theta_5)\left(\cos(\theta_3)\cos\left(\theta_2+\frac{\pi}{2}\right)-\sin(\theta_3)\sin\left(\theta_2+\frac{\pi}{2}\right)\right)\right)+l_5\left(\sin(\theta_3)\sin\left(\theta_2+\frac{\pi}{2}\right)-\cos(\theta_3)\cos\left(\theta_2+\frac{\pi}{2}\right)\right)+$$
$$l_4\sin(\theta_3)\cos\left(\theta_2+\frac{\pi}{2}\right)+l_4\cos(\theta_3)\sin\left(\theta_2+\frac{\pi}{2}\right)+l_3\sin\left(\theta_2+\frac{\pi}{2}\right)+l_1$$

And

$[n_x\ n_y\ n_z]$: The unit vector indicates the direction of the X-axis at the robot end tip to the base coordinate system.

$[o_x\ o_y\ o_z]$: The unit vector indicates the direction of the Y-axis at the robot end tip to the base coordinate system.

$[a_x\ a_y\ a_z]$: The unit vector indicates the direction of the Z-axis at the robot end tip to the base coordinate system.

After computing the forward kinematics of the robotic manipulator, which resulted in the end-effector's transformation matrix, it was essential to determine the orientation of the end-effector in a more intuitive manner. To achieve this, Euler angles were extracted, providing a clear representation of the orientation through three sequential rotations about the coordinate axes. Specifically, using the $ZY'X''$ Euler angle convention, the orientation was described by a yaw (ψ) about the Z-axis, followed by a pitch (θ) about the Y-axis, and finally a roll (ϕ) about the X-axis, Figure 3.7.

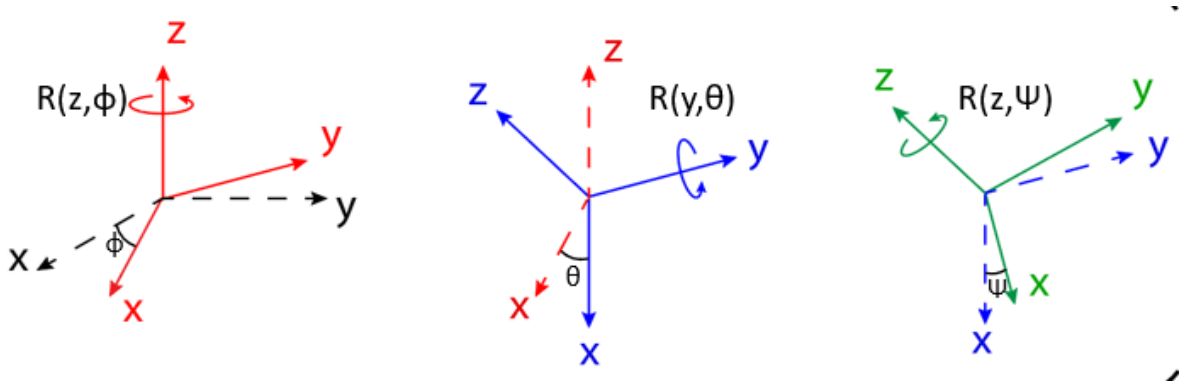

Figure 3.7: $z\ y'x''$ Euler rotation angles

These angles were obtained from the rotation matrix component of the forward kinematics matrix, effectively characterizing the spatial orientation of the end-effector and are given by;

$$\begin{aligned} \psi &= atan2d(o_x, n_x) \\ \theta &= atan2d(-a_x, \sqrt{{a_y}^2 + {a_z}^2}) \\ \phi &= atan2d(a_y, a_z) \end{aligned} \tag{3.4}$$

With the development of the forward kinematic model for the 6-DOF robot, a custom function block, Figure 3.8, was created in MATLAB Simulink for integration into the joint-space controller. This function block allows for seamless implementation of the forward kinematics within the control architecture, enabling precise calculation of the end-effector's position and orientation during simulation.

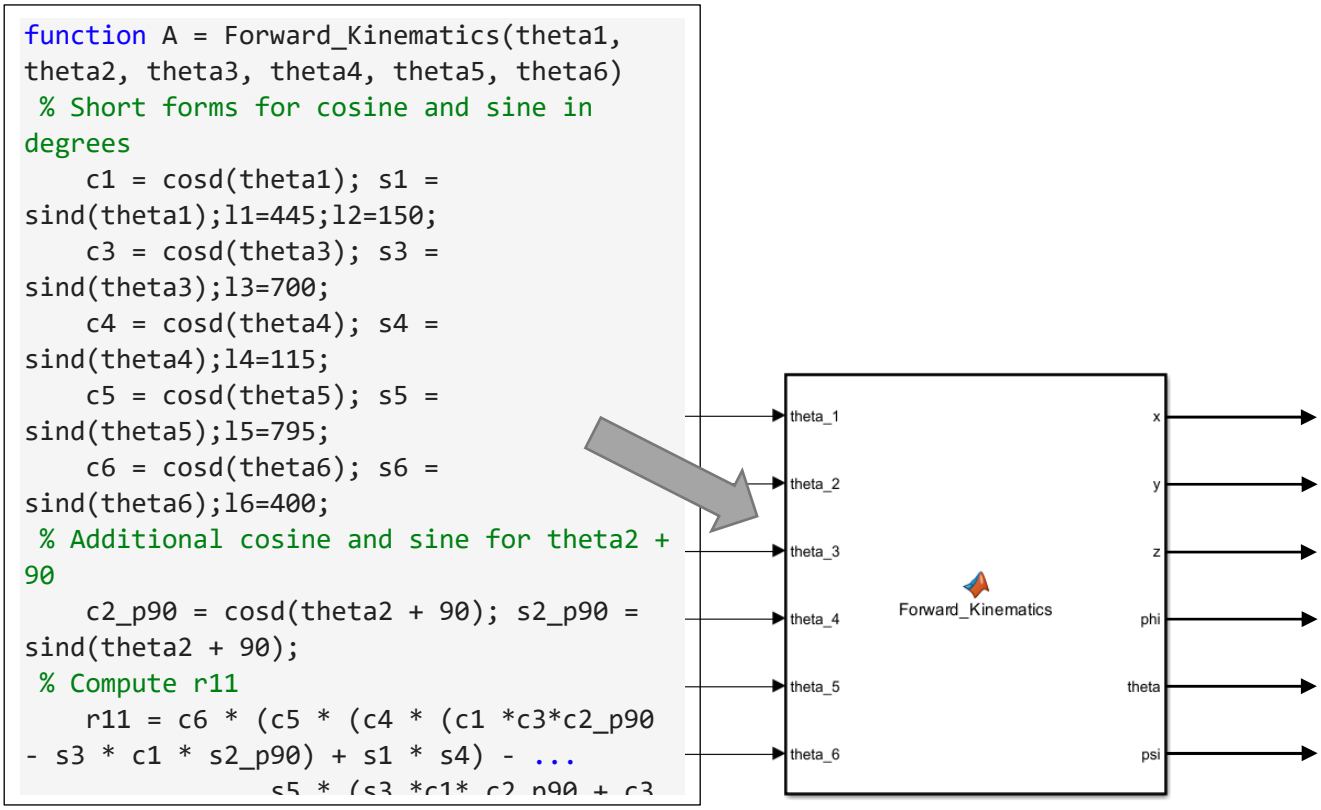

Figure 3.8: Forward kinematics Simulink model function block

3.2.2. Inverse Kinematics

Inverse kinematics is the process of calculating the joint angles needed to position and orient a robot's end-effector at a desired location. In a joint-space control architecture, inverse kinematics is essential because it translates the desired end-effector movements into specific joint commands, enabling precise control of the robot's motion. Inverse kinematics is inherently complex, especially for 6-DOF robots, due to the multiple degrees of freedom that result in redundancy and multiple potential solutions. In most cases, the problem presents more than two solutions, making it challenging to determine the optimal joint angles for a given end-effector position and orientation.

To address this complexity, various analytical, geometrical, and numerical methods have been developed.

If certain requirements are met, kinematic decoupling provides the simplest method for solving the inverse kinematics of higher-DOF robots. These key requirement for achieving this simplification is that the robot must feature a spherical wrist characterized by [57], [58], [59]:

- The last three rotational axes of the robot should intersect at a single point, facilitating the decoupling of orientation and positioning tasks
- At least three of the rotational axes must be parallel, ensuring that the orientation of the end-effector can be controlled independently from its position.

Since the 6-DOF robot meets the key requirements of having a spherical wrist, its inverse kinematics were solved through kinematic decoupling. The 6-DOF robot was decoupled into two distinct segments: the first three joints for positioning and the last three joints for orientation, Figure 3.9. The first segment, consisting of the initial three joints, was designated for controlling the robot's position in space.

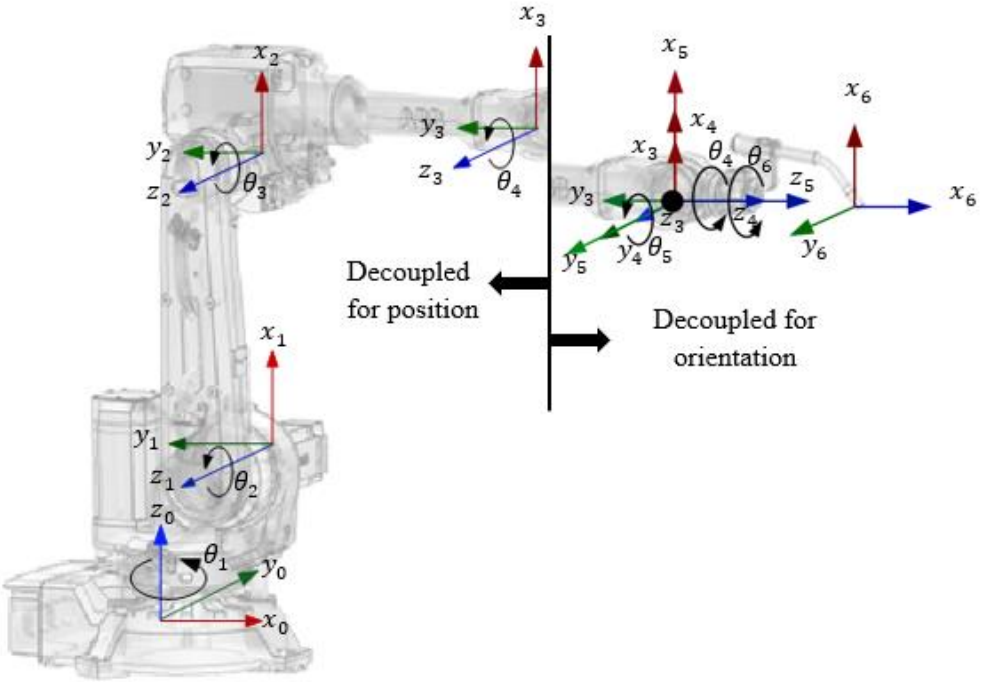

Figure 3.9: Kinematic decoupling of the 6 DOF robot

These joints determine the location of the end-effector by adjusting its x, y, and z coordinates. The second segment, comprising the last three joints, was responsible for controlling the orientation of

the end-effector. This decoupling allowed for a more straightforward approach to solving the inverse kinematics by addressing the positioning and orientation tasks independently, leveraging the spherical wrist configuration to isolate and solve each part separately. This approach facilitated a more manageable solution process by separating the positioning and orientation tasks, simplifying the otherwise intricate inverse kinematics problem[57], [59], [60], [61].

Prior to decoupling the robot into two independent sections, the position of the wrist was computed based on the end-effector's position. This step was crucial as it provided the necessary coordinates for the wrist center, which serves as the pivotal point for separating the tasks of positioning and orientation in the kinematic analysis.

The position of the end-effector is given by $[P_x\,, P_y\,, P_z\,]^T$ and since the end effector is located about d_6 along the z direction from the wrist position; the wrist position, $[W_x\,, W_y\,, W_z\,]^T$, is given by:

$$W = \begin{bmatrix} W_x \\ W_y \\ W_z \end{bmatrix} = \begin{bmatrix} p_x \\ p_y \\ p_z \end{bmatrix} - d_6 \begin{bmatrix} r_{11} & r_{12} & r_{13} \\ r_{21} & r_{22} & r_{32} \\ r_{31} & r_{23} & r_{33} \end{bmatrix} \begin{bmatrix} 0 \\ 0 \\ 1 \end{bmatrix} \tag{3.5}$$

Hence;

$$W = \begin{bmatrix} w_x \\ w_y \\ w_z \end{bmatrix} = \begin{bmatrix} P_x - d_6 r_{13} \\ P_y - d_6 r_{23} \\ P_z - d_6 r_{33} \end{bmatrix} \tag{3.6}$$

With the wrist position known, the first three joints were solved from the first section of the robot, Figure 3.10, algebraically;

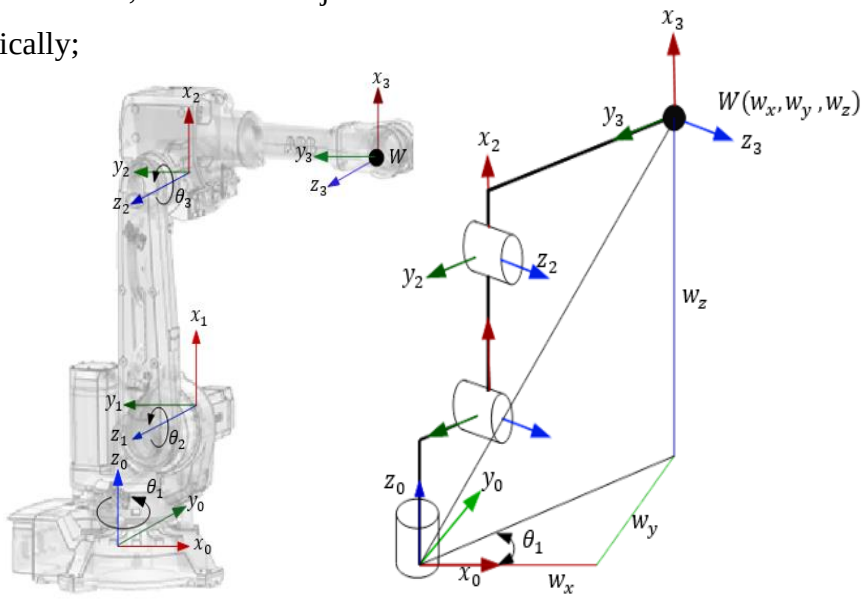

Figure 3.10: Section one Decoupled for position

Using the wrist center coordinates, θ_1 was calculated by projecting the wrist center onto the base plane, Figure 3.10, and was found to be;

$$\theta_1 = atan2(w_y, w_x) \tag{3.7}$$

To solve for the two angles θ_1 and θ_2, the position of the wrist center (denoted as P_4^0) relative to the frame $\{1\}$ was first computed. This was achieved by subtracting the position vector from, giving the transformation from frame 1 to frame 4. This transformation simplifies the geometric calculations required to determine the joint angles by isolating the effective position of the wrist center.

$$P_4^1 = P_4^0 - P_1^0 \tag{3.8}$$

The position of $\{1\}$ relative to the base frame, $\{0\}$, is given by;

$$P_1^0 = \begin{bmatrix} a_1 cos\theta_1 \\ a_1 sin\theta_1 \\ d_1 \end{bmatrix} \tag{3.9}$$

And the position of the wrist relative to the base frame is given by;

$$P_4^0 = W = \begin{bmatrix} w_x \\ w_y \\ w_z \end{bmatrix} = \begin{bmatrix} P_x - d_6 r_{13} \\ P_y - d_6 r_{23} \\ P_z - d_6 r_{33} \end{bmatrix} \tag{3.10}$$

Hence, the position of the wrist relative to the position of frame $\{1\}$ was found to be;

$$P_4^1 = \begin{bmatrix} P_x - d_6 r_{13} - a_1 cos\theta_1 \\ P_y - d_6 r_{23} - a_1 sin\theta_1 \\ P_z - d_6 r_{33} - d_1 \end{bmatrix} \tag{3.11}$$

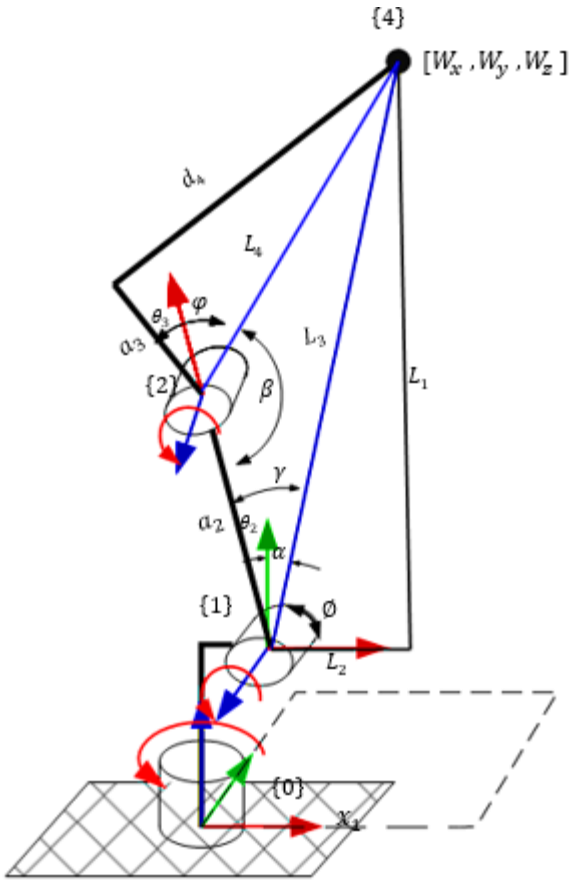

Figure 3.11: Kinematic chain of the first section

The joint angles θ_2 and θ_2 were calculated using geometric techniques, specifically by applying the law of cosines to a triangle formed by the robot's three links and found to be:

$$\theta_2 = \gamma + \emptyset - 90$$
$$\theta_3 = \beta + \varphi - \pi \quad (3.12)$$

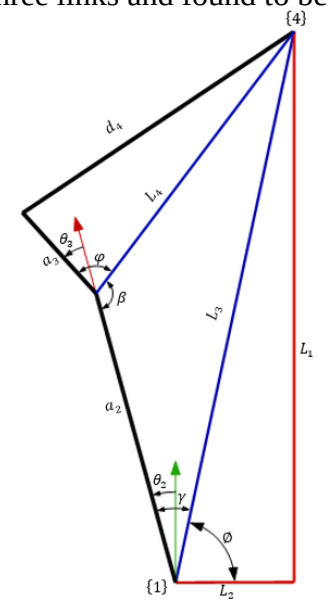

Where:

$$\gamma = cos^{-1}\left(\frac{{a_2}^2 + {L_3}^2 - {L_4}^2}{2a_2 L_3}\right)$$

$$\beta = cos^{-1}\left(\frac{{a_2}^2 + {L_4}^2 - {L_3}^2}{2a_2 L_4}\right)$$

$$\varphi = tan^{-1}\left(\frac{d_4}{a_3}\right)$$

$$L_1 = P_4^1[3] = P_z - d_6 r_{33} - d_1$$

$$L_3 = \sqrt{[P_4^1]'[P_4^1]}$$

$$L_4 = \sqrt{{a_3}^2 + {d_4}^2}$$

$$L_2 = \sqrt{(P_x - d_6 r_{13} - a_1 cos\theta_1)^2 + (P_y - d_6 r_{23} - a_1 sin\theta_1)^2}$$

To solve for the remaining three joint angles, the second segment of the decoupled robot, Figure 3.12, which focuses on orientation, was used. This part of the inverse kinematics computation considers the orientation of the end-effector, allowing the calculation of θ_4 , θ_5, and θ_6 by using the rotational part of the transformation matrix, where the orientations were matched to achieve the desired pose of the end-effector.

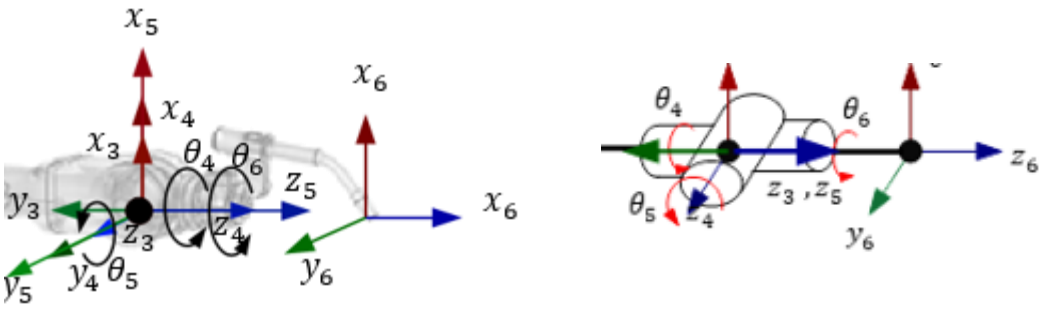

Figure 3.12: The second segment of the decoupled robot

The rotation matrix from the wrist to the end-effector orientation was computed by multiplying the three successive transformations from {3} to {6}. By extracting the rotational part of the homogeneous transformation matrix, the rotation matrix, R_6^3 was obtained and is given by:

$$R_6^3 = \begin{bmatrix} C_4C_5C_6 - S_4S_6 & -S_6C_4C_5 - S_4C_6 & S_5C_4 \\ S_4C_5C_6 + S_6C_4 & -S_4S_6C_5 + C_4C_6 & S_4S_5 \\ -S_5C_6 & S_5S_6 & C_5 \end{bmatrix} \quad (3.13)$$

From the forward kinematics of the robot, the rotation matrix of the end-effector relative to the wrist, R_6^3 is given by:

$$R_6^3 = [R_3^0]^{-1} R_6^0 \quad (3.14)$$

This matrix represents the orientation of the end-effector frame relative to the wrist frame and is obtained from the product of the individual transformation matrices from the wrist to the end-effector. And the orientation of the end effector relative to the base is given by:

$$R_6^0 = \begin{bmatrix} r_{11} & r_{12} & r_{13} \\ r_{21} & r_{22} & r_{23} \\ r_{31} & r_{32} & r_{33} \end{bmatrix} \tag{3.15}$$

And the orientation of the wrist relative to the base of the robot, R_3^0 is given by:

$$R_3^0 = \begin{bmatrix} C_1C_{23} & S_1 & C_1S_{23} \\ S_1C_{23} & -C_1 & S_1S_{23} \\ S_{23} & 0 & -C_{23} \end{bmatrix} \tag{3.16}$$

Using equation (3.14) the rotational matrix R_6^3 is given by;

$$R_6^3 = \begin{bmatrix} r_{11}C_1C_{23} + r_{21}S_1C_{23} + r_{31}S_{23} & r_{12}C_1C_{23} + r_{22}S_1C_{23} + r_{23}S_{23} & r_{13}C_1C_{23} + r_{32}S_1C_{23} + r_{33}S_{23} \\ r_{11}S_1 - r_{21}C_1 & r_{12}S_1 - r_{22}C_1 & r_{13}S_1 - r_{32}C_1 \\ r_{11}C_1S_{23} + r_{21}S_1S_{23} & r_{12}C_1S_{23} + r_{22}S_1S_{23} - r_{23}C_{23} & r_{13}C_1S_{23} + r_{32}S_1S_{23} - r_{33}C_{23} \end{bmatrix}$$

By equating the rotational matrices, the values for the last three joints were determined to be:

$$\begin{aligned} \theta_4 &= atan2(r_{13}S_1 - r_{32}C_1, r_{13}C_1C_{23} + r_{32}S_1C_{23} + r_{33}S_{23}) \\ \theta_5 &= atan2\left(\sqrt{(r_{13}C_1C_{23} + r_{32}S_1C_{23} + r_{33}S_{23})^2 + (r_{13}S_1 - r_{32}C_1)^2}, r_{13}C_1S_{23} + r_{32}S_1S_{23} - r_{33}C_{23}\right) \\ \theta_6 &= atan2(r_{12}C_1S_{23} + r_{22}S_1S_{23} - r_{23}C_{23}, -(r_{11}C_1S_{23} + r_{21}S_1S_{23})) \end{aligned} \tag{3.17}$$

Similar to the forward kinematics custom Simulink function block, a custom Simulink function block for inverse kinematics was also developed. This block was programed based on the derived inverse kinematics equations, taking into account the joint limits of each joint and the workspace constraints of the robot. This function block ensures that the calculated joint angles remain within feasible ranges, allowing the robot to achieve the desired end-effector positions and orientations while adhering to its mechanical limitations.

3.3. Sample Trajectory Design

A trajectory is a predefined path that guides a robot's end-effector, typically defined by position, orientation, velocity, and acceleration over time. In robotic control, the trajectory serves as a reference, ensuring precise movement to achieve specific tasks [62][63]. Developing a sample trajectory function is crucial for testing and validating the kinematic model and controller. By simulating a realistic path, this function helps assess the robot's ability to follow the desired trajectory, confirming that the control system is correctly tuned for optimal performance[64][65]. To test the kinematic models and the controller's performance a sample circular trajectory function was developed with the robot's workspace, Figure 3.13, and the specific technical requirements for welding in mind [66]. Figure 3.13

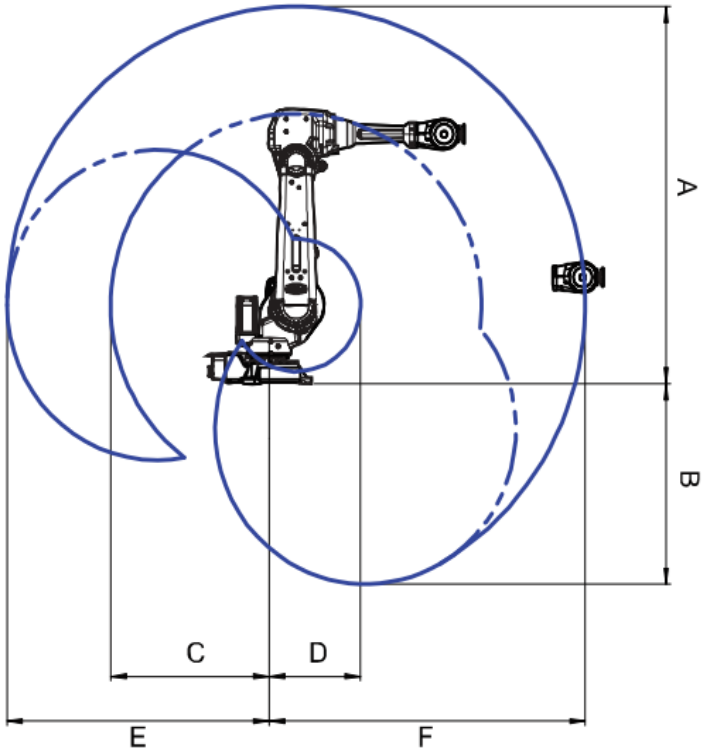

Position	Distance
Pos. A	1948mm
Pos. B	993mm
Pos. C	837mm
Pos. D	469mm
Pos. E	1353mm
Pos. F	1653 mm

Figure 3.13: Workspace of the Robot

One of the most common and challenging types of welding tasks is large circular welding. This involves welding around a larger cylindrical object, which requires maintaining a consistent angle and precise control of the torch along a curved path. Such circular trajectories are often used in

applications such as pipe welding, pressure vessels, and other cylindrical components where a continuous and seamless weld is essential. The complexity arises from the need to maintain the correct orientation of the welding torch throughout the circular path, ensuring that the weld quality remains consistent. Hence, circular a trajectory was selected and developed for evaluating the kinematic, dynamic model, and controller performance of the robot. Although the shape, position, orientation, and associated parameters of the trajectory may vary depending on the specific application, this circular trajectory serves as an effective baseline.

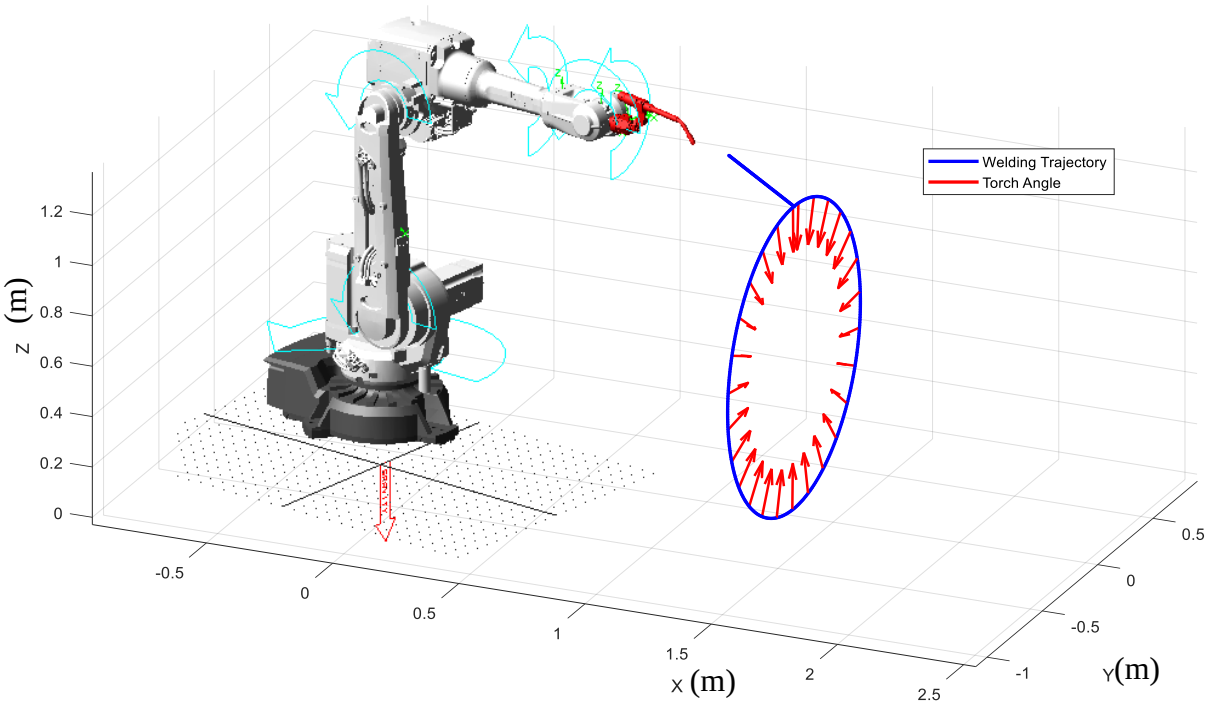

Figure 3.14: 3D Trajectory with end effector orientation

The trajectory is defined with a fixed center at coordinates (1345, 0, 600) in the x, y, and z directions, respectively. The robot's end-effector follows a circular path in the *zy*-plane, with a radius of 600mm. This trajectory was designed not only with position but also with orientation in mind, recognizing that successful welding operations require the torch to maintain a specific angle relative to the surface. In most cases, this angle is 45 degrees[67]. Accordingly, the orientation of the end-effector was designed to consistently maintain a 45-degree angle, pointing towards the center of the circular path, ensuring optimal welding conditions throughout the operation. Even though the velocity of the end-effector to complete each trajectory varies depending on the

application and may not match this assumption, for this simplified simulation, the time required to complete the trajectory was limited to 15 seconds. This trajectory has three main phases:

- Movement from Home Position to the Starting Welding Position
- Circular Welding Path
- Return to Home Position

The overall trajectory begins by moving the robot's end-effector from its home position to the starting point of the welding operation over a period of 1 sec and remain there for 0.5 sec preparing for welding. Once the end-effector reaches the designated welding position and preparations are done, the robot initiates the welding process, guiding the torch around the circular path while maintaining an effective torch angle towards the center of the circular trajectory for a period of 8.5 sec. After completing the weld, the trajectory ensures a smooth and controlled return of the end-effector back to its original home position, completing the welding task. After completing the given welding trajectory, the robot stops for 0.5 sec in the to finalize the welding process and the move back to its home position within the last 1 sec of the overall trajectory finalizing the sample trajectory chosen for testing the developed kinematic, dynamic models and the design controller of the robot. By keeping those parameters in mind, a pricewise function of the trajectory was developed.

$$x(t) = \begin{cases} 302t + 1043\,, & 0 \le t < 1 \\ 1345, & 1 \le \mathrm{t} < 1.5 \\ 1345, & for\ 1.5 \le \mathrm{t} < 10 \\ 1345, & for\ 10 \le \mathrm{t} < 10.5 \\ 1345 - 302t, & for\ 10.5 \le \mathrm{t} < 11.5 \end{cases}$$

$$y(t) = \begin{cases} 300t + 1045\,, & for\ \ 0 \le t < 1 \\ 1345, & for\ 1 \le \mathrm{t} < 1.5 \\ 15467.5 - 300\sin(t), & for\ 1.5 \le \mathrm{t} < 10 \\ 15467.5 - 300\sin(t), & for\ 10 \le \mathrm{t} < 10.5 \\ 15467.5 - 300\sin(t), & for\ 10.5 \le \mathrm{t} < 11.5 \end{cases} \qquad (3.18)$$

$$z(t) = \begin{cases} 300t + 1045\,, & for\ \ 0 \le t < 1 \\ 1345, & for\ 1 \le \mathrm{t} < 1.5 \\ 15467.5 - 300\cos(t), & for\ 1.5 \le \mathrm{t} < 10 \\ 15467.5 - 300\cos(t), & for\ 10 \le \mathrm{t} < 10.5 \\ 15467.5 - 300\cos(t), & for\ 10.5 \le \mathrm{t} < 11.5 \end{cases}$$

3.4. Dynamic Modeling of the 6 DOF Robot

Dynamic modeling in robotics involves creating mathematical representations of the forces and torques affecting a robot to predict its behavior under various conditions. This includes forward dynamics, which calculates the robot's motion based on known forces and torques, and inverse dynamics, which determines the required forces and torques to achieve a desired motion. Integrating both models into the control loop is essential for optimizing a robot's performance, enabling precise control and accurate execution of complex tasks across diverse applications.

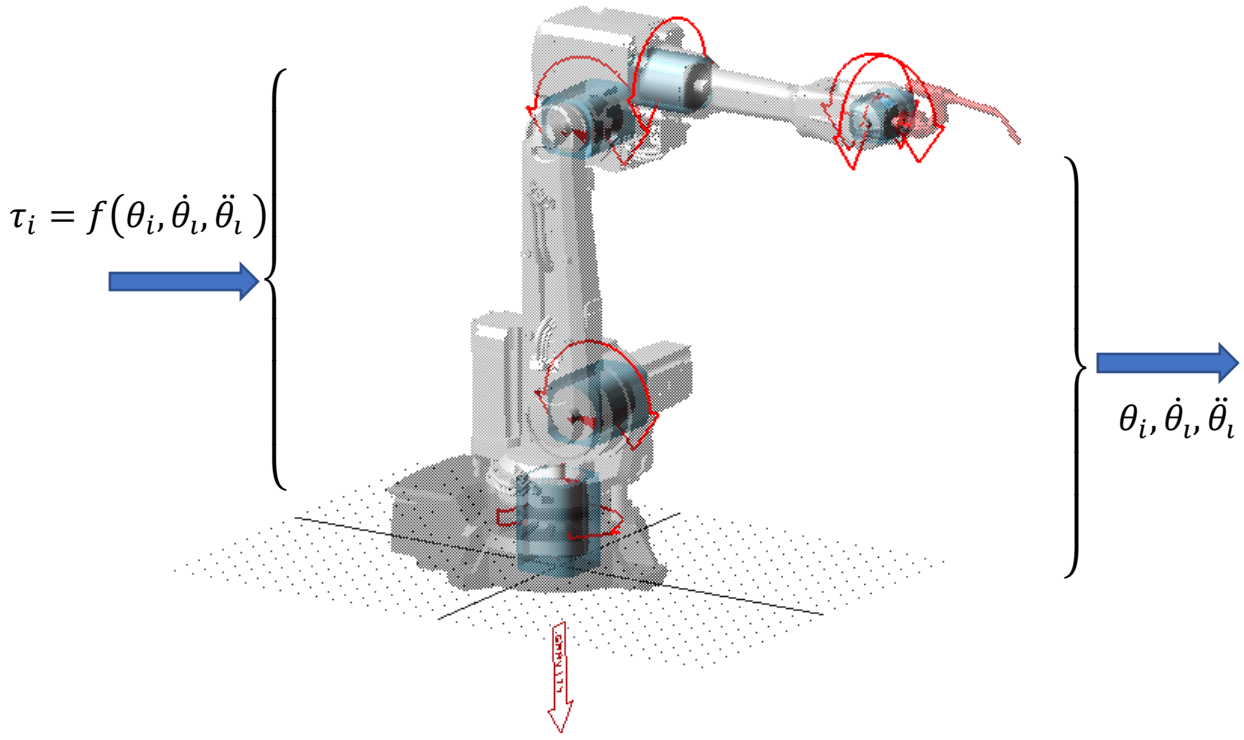

Figure 3.15: Actuator model included inverse dynamic model of the robot

In the design of control systems, integrating the inverse dynamic model is crucial for determining the forces and torques required to achieve specified motions. Analytical methods, such as the Euler-Lagrange and Newton-Euler approaches, are often employed to derive these dynamic models, providing a structured framework to understand the robot's dynamic behavior. However, for robots with more than 3DOF, the complexity of analytically developing the dynamic model increases significantly. Therefore, for the 6-DOF welding robot, the dynamic model was developed by integrating advanced SolidWorks, MSC Adams, and MATLAB/Simulink. This integration

allows for comprehensive simulation and analysis, ensuring the dynamic model's accuracy and facilitating precise control and optimization of the robot's performance across a range of applications.

3.5. Controller Design

The development of advanced control systems for industrial robots is critical to achieving precision, efficiency, and adaptability in manufacturing processes. While PID controllers are widely used for their simplicity and effectiveness, they often struggle with the non-linearities and uncertainties inherent in robotic systems[68]. To address these challenges, ANFIS-PID controllers have emerged as a promising solution, combining the learning capabilities of neural networks with the interpretability of fuzzy logic to create more robust and adaptive control strategies [42], [69]. By integrating ANFIS with the PID framework, the controller aims to enhance trajectory tracking, minimize errors, and adapt to varying loads and environmental conditions. This approach seeks to overcome the limitations of traditional PID controllers, demonstrating the potential of ANFIS-PID to improve the operational performance of the ABB IRB 2600 and contribute to advancements in intelligent robotic control systems.

Before delving into the controller design, it is essential to understand the functional requirements of the ABB IRB 2600 robot and the closed-loop control architecture necessary for its precise operation. The functional requirements of the robot's control system include:

- Accurate Trajectory Tracking: Ensuring the robot's end-effector follows the desired path with minimal error.
- Robustness to Disturbances: Maintaining performance despite changes in payload, environmental conditions, or external disturbances.
- Adaptability: Adjusting to varying operating conditions, including different tasks and load configurations.
- Minimization of Overshoot and Settling Time: Achieving smooth and stable motion without significant deviations or delays.

While PID controllers are widely used for their simplicity and effectiveness in simpler industrial applications, their limitations become apparent when controlling complex, dynamic, and non-linear robotic systems like the ABB IRB 2600. These challenges include difficulty in managing varying payloads, handling non-linearities in the robot's kinematics and dynamics, and optimizing

multiple objectives such as precision, stability, and adaptability under changing conditions. Additionally, traditional PID controllers often struggle to reject both internal disturbances, such as joint friction, and external disturbances, such as unexpected forces or environmental changes. To meet the stringent functional requirements for precise trajectory tracking, robustness, and adaptability, it is crucial to address these limitations. Considering the non-linear and uncertain nature of the robotic system, an ANFIS was integrated into the PID framework. This hybrid approach enhances the controller's ability to adapt to dynamic conditions, improve time response, and effectively handle disturbances, ensuring the robot's performance remains optimal across varying operational scenarios.

3.5.1. Design of ANFIS-PID controller for position and orientation control

To achieve effective and robust control of the ABB IRB 2600 robot, addressing the inherent challenges posed by system non-linearities, parametric uncertainties, and varying payload conditions is imperative. In response to these complexities, a feed-forward ANFIS-PID controller was developed as a sophisticated solution. The ANFIS-PID controller combines the complementary strengths of fuzzy logic systems, artificial neural networks, and traditional PID control, offering a powerful approach to manage the intricate dynamics of robotic control applications. The fuzzy logic component, based on a rule-based architecture, allows the ANFIS controller to encode human-interpretable knowledge about the robot's dynamic behavior, capturing complex relationships and dependencies in a structured, adaptable framework. Simultaneously, the neural network component enables the controller to learn from data and generalize to new situations, adapting to non-linear behaviors and uncertain operating conditions. The integration of the ANFIS model with the PID controller enhances the system's capability for precise trajectory tracking, improved robustness against external disturbances, and adaptability to fluctuating operational parameters such as varying payloads or environmental influences. By addressing the limitations of traditional PID controllers, particularly their inability to effectively handle non-linearities and multi-objective optimization requirements, the feed-forward ANFIS-PID controller offers a more resilient and adaptive solution. Its capacity for real-time adaptation and disturbance rejection makes it especially well-suited for industrial applications where precision, reliability, and efficiency are critical.

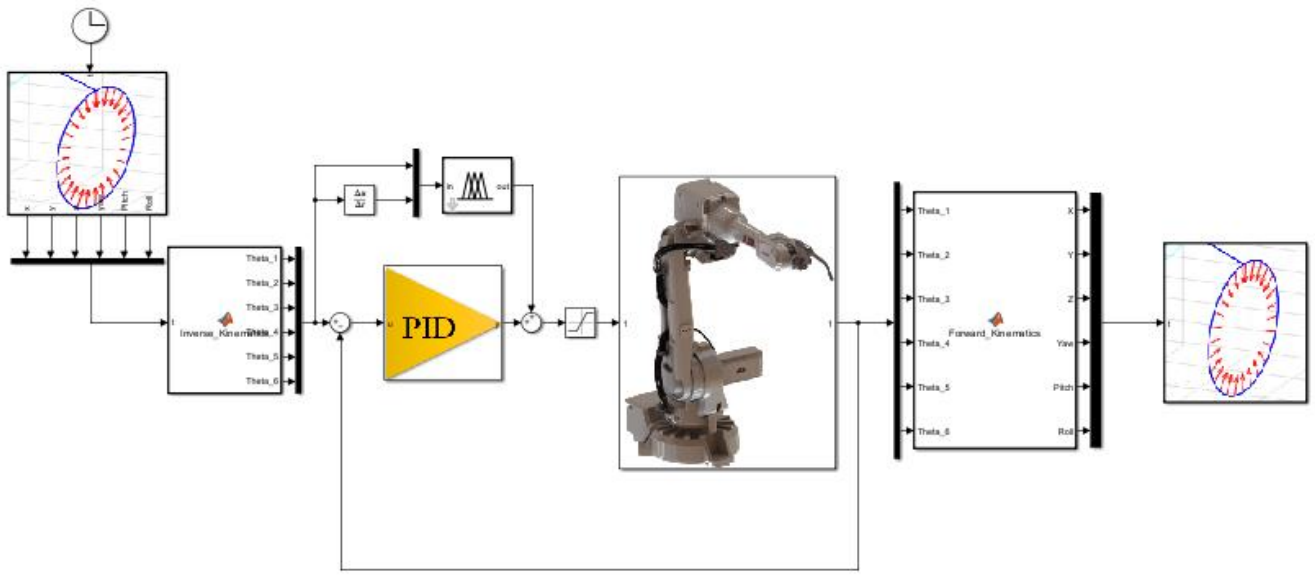

Figure 3.16: ANFIS-PID controller Architecture of ABB robot

3.5.2. Architecture of the ANFIS controller

The architecture of the ANFIS controller is designed with a structured approach that combines both structure learning and parameter learning to optimize its performance. Initially, the structure learning phase identifies appropriate fuzzy logic rules, while the parameter learning phase refines membership functions and other key parameters [35]. This iterative learning process ensures that both the structural framework and internal parameters of the controller are adapted to best suit the specific control task.

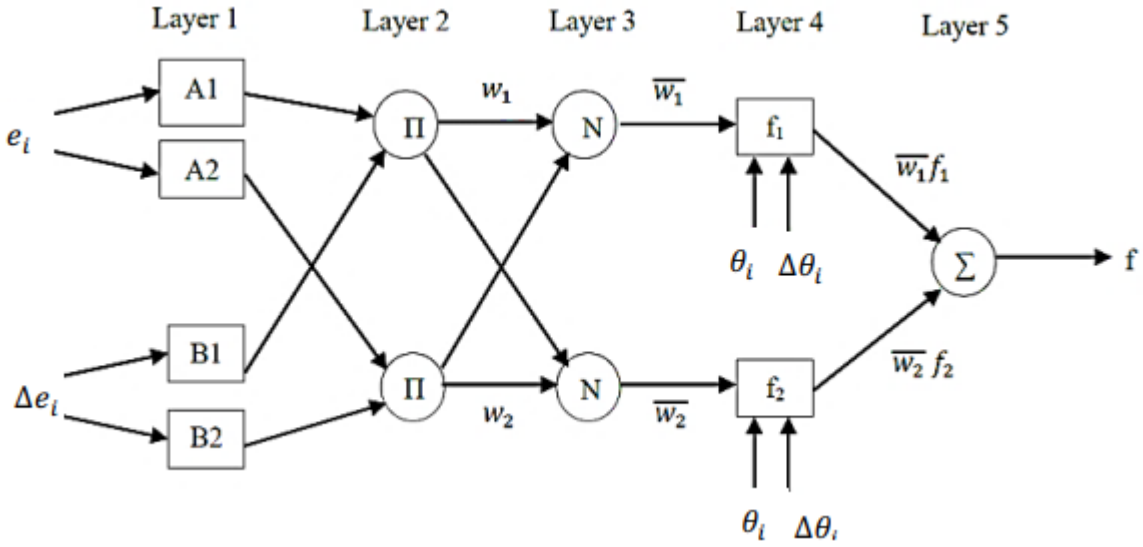

Figure 3.17: ANFIS controller Architecture

The ANFIS architecture consists of five layers, as shown in Figure 3.17. The first and fourth layers contain adaptive nodes, allowing for dynamic adjustment of parameters, while the other layers consist of non-adaptive nodes, maintaining the stability and robustness of the overall system [34]. This combination of adaptability and stability enhances the controller's performance, making it effective in handling complex control tasks.

Layer 1 (Fuzzification): Each input node in this layer is an adaptive node which produce membership grade of linguistic label.

$$O_{1,i} = \mu_{A_i}(e), for\ i = 1,2 \ldots\ldots j$$
$$O_{1,i} = \mu_{B_{i-2}}(\Delta e), for\ i = 3,4 \ldots \text{j} \tag{3.19}$$

Where:

- e, and Δe are the inputs
- A_i and B_{i-2} are the fuzzy sets whereas
- μ_{A_i} and $\mu_{B_{i-2}}$ Represents the degree of membership.

Considering the controller's two inputs and one output, a Sugeno fuzzy model with linear Gaussian membership functions was chosen due to its computational efficiency and versatility [69], [70], [71]. Sugeno fuzzy inference, also known as Takagi-Sugeno-Kang inference, utilizes singleton output membership functions that can either be constant or linear functions of the input variables. In Sugeno systems, the defuzzification process is more computationally efficient because it involves a weighted average or weighted sum of a few data points, in contrast to the Mamdani system, which requires calculating the centroid of a two-dimensional area, Figure 3.18.

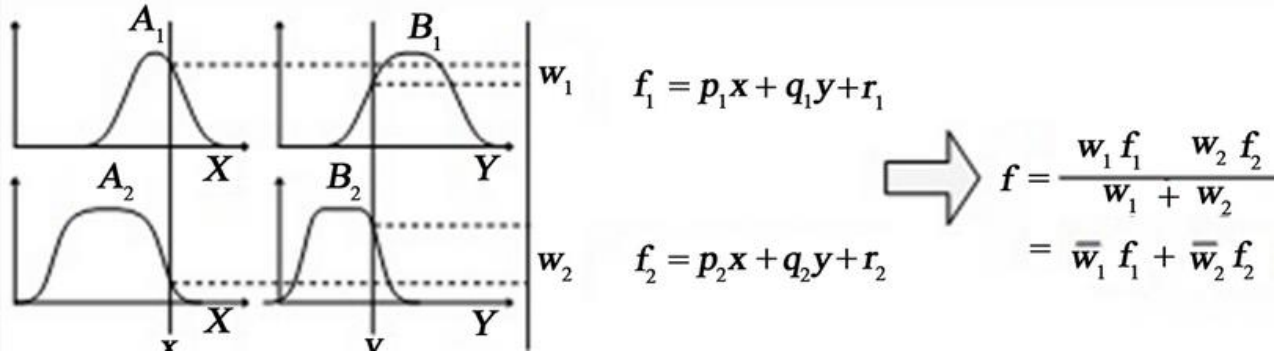

Figure 3.18: Segeno fuzzy inference system

The general format of the rule for the Sugeno fuzzy method is:

$$\text{If } x \text{ is } A \text{ AND } y \text{ is } B \text{ THEN } z \text{ is } f(x,y) \tag{3.20}$$

Where:

- x, y, and z are linguistic variables;
- A and B are fuzzy sets; and
- $f(x,y)$ is the mathematical function.

Considering, the computational complexity of the ANFIS, the number of membership functions of each node was limited to only 10, Figure 3.19.

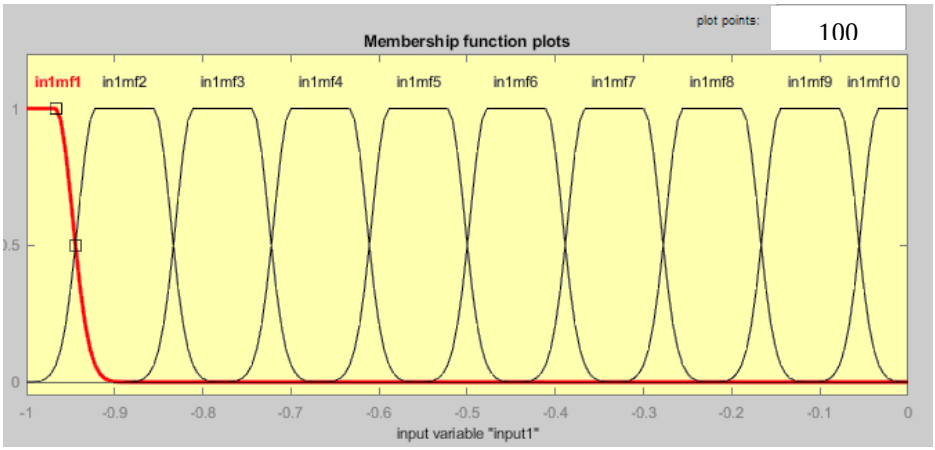

Figure 3.19 : Input Membership function of the ANFIS

Layer 2 (Product): All the nodes within this layer are constant and signify the activation level for each rule. The node's output is determined by multiplying the incoming signals into the node and forwarding the result to the subsequent node.

$$O_{2,i} = W_i = \mu A_i(e)\mu B_{i-2}(\Delta e) \text{ for } i = 1,2 \ldots . j^2 \tag{3.21}$$

Where:

- w_i Represents the firing strength for each rule.

Layer 3 (Normalization): ach node in this layer represents a fuzzy rule. The firing strength of a rule is computed using the fuzzy AND operation, typically the product of membership values from the

fuzzification layer. The output of the node is the outcome of multiplying the signals coming into the node and carried out to the next node.

$$O_{3,i} = \overline{w_i} = \frac{w_i}{w_1 + w_2}, i = 1,2. \tag{3.22}$$

Layer 4 (Defuzzification): Every node i in this layer is the adaptive node at which their values are given by a node function of:

$$O_{3,i} = \overline{w_i} f_i = \overline{w_i}(p_i e + q_i \Delta e + r_i) \tag{3.23}$$

Where:

- $\overline{w_i}$ is the normalized filtering strength computed from layer 3
- p_i, $q_{i,}$ and r_i are the consequent parameters of the specific node.

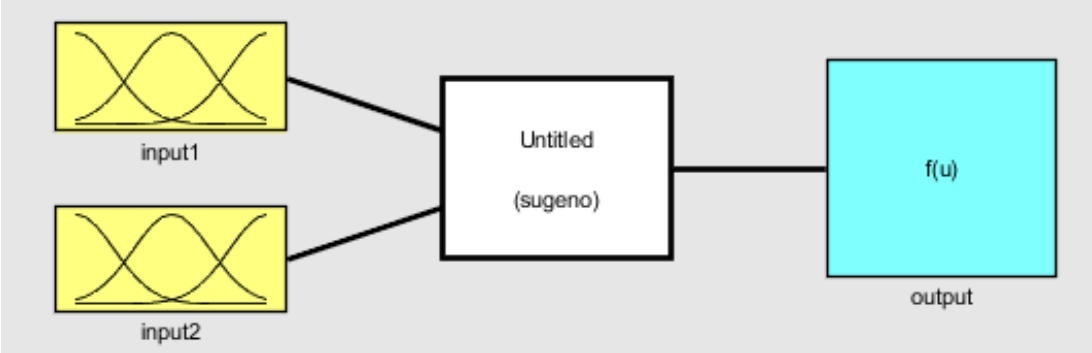

Figure 3.20 : Defuzzification of the Sugeno fuzzy Inference system of the ANFIS

In this layer at which their values are updated during the learning process of the ANFIS.

Layer 5 (output): This final single nodded layer labeled by Σ computes the overall output of the ANFIS controller

$$O_{5,i} = \overline{w_i} f_i = \frac{\sum_{i=1}^{j^2} w_i f_i}{\sum_{i=1}^{j^2} w_i} \tag{3.24}$$

To train the ANFIS, a hybrid method was employed, combining least-squares estimation for the parameters linked to the output membership functions with the backpropagation gradient descent algorithm for the parameters related to the input membership functions[35], [72]. This hybrid approach ensures effective optimization by leveraging the strengths of both techniques to fine-tune the model's parameters and improve its overall performance. The least-squares method is used to

adjust the output membership functions, while the backpropagation method refines the input membership functions, resulting in a robust and adaptive controller.

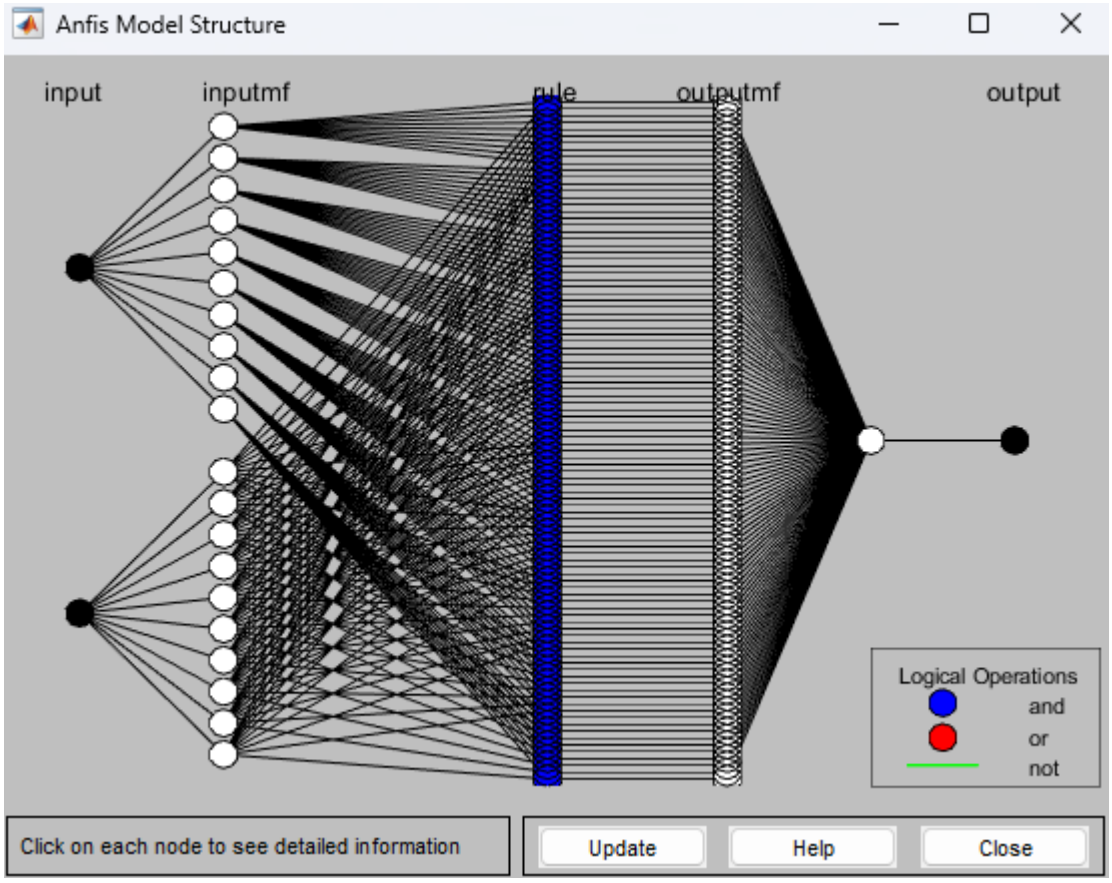

Figure 3.21: Structure of the 10x10 MF FIS

3.5.3. Training and Testing of the ANFIS

To train the ANFIS-PID controller, a traditional PID controller was initially designed as a baseline, Figure 3.22. Training and testing data were then collected from the PID controller's operation under various conditions to provide a comprehensive dataset for the ANFIS model. A set of 1301 data points was used, considering the computational resources allocated for this research. This dataset was carefully selected to ensure a balance between the complexity of the control task and the available computational capacity, enabling efficient training while maintaining the quality of the model's performance. The collected data included input-output pairs representing different system states and control responses, which were essential for fine-tuning the fuzzy logic and neural network components of the ANFIS.

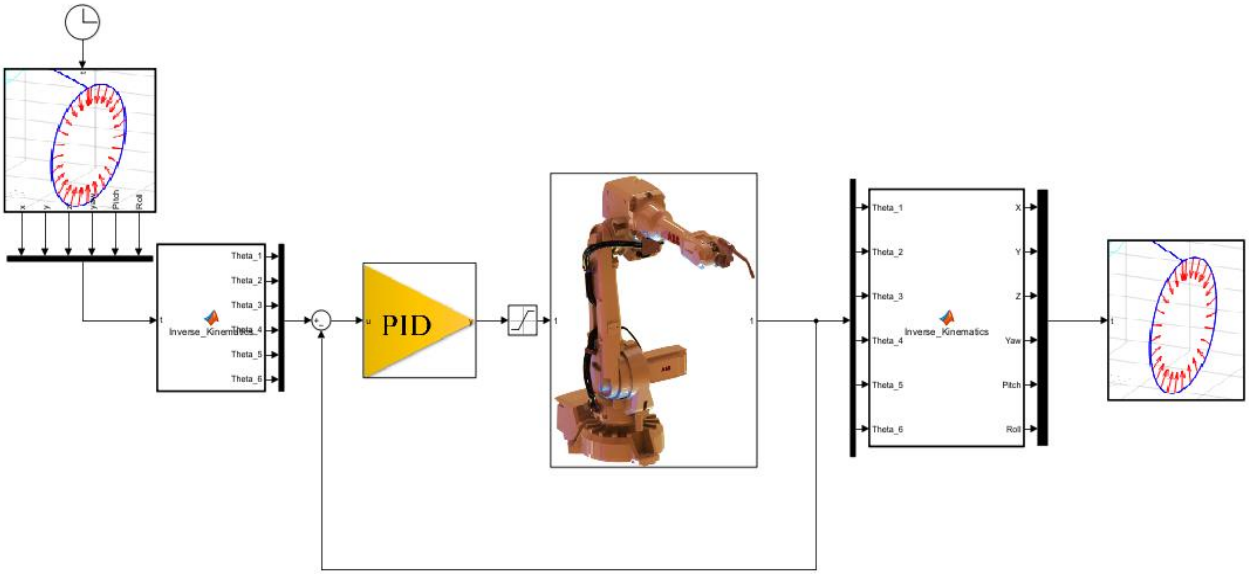

Figure 3.22: Set of PID controllers developed in order to train the ANFIS

A set of training data was gathered for each ANFIS controller, and a fuzzy inference system was constructed based on the data acquired from the PID controllers for both joints. This system was developed following the configuration outlined in Table 3.2.

Table 3.2: ANFIS Training Parameters

Minimal training RMSE	0.00296842
Number of nodes:	245
Number of linear parameters:	300
Number of nonlinear parameters:	80
Total number of parameters:	380
Number of training data pairs:	13001
Number of checking data pairs:	13001
Number of fuzzy rules:	100

Using the training data collected from each of the PID controllers, the inference system of the ANFIS-PID controller was trained, and the training error for each of the joint controllers is presented in Figure 3.23. This outcome was obtained by employing 10 linear Gaussian membership functions and performing 4 iterations of 20 epochs using the hybrid optimization

model [34], [73]. The training process ensured that the controller effectively adapted to the system's dynamics, improving its accuracy and performance in controlling the robotic joints.

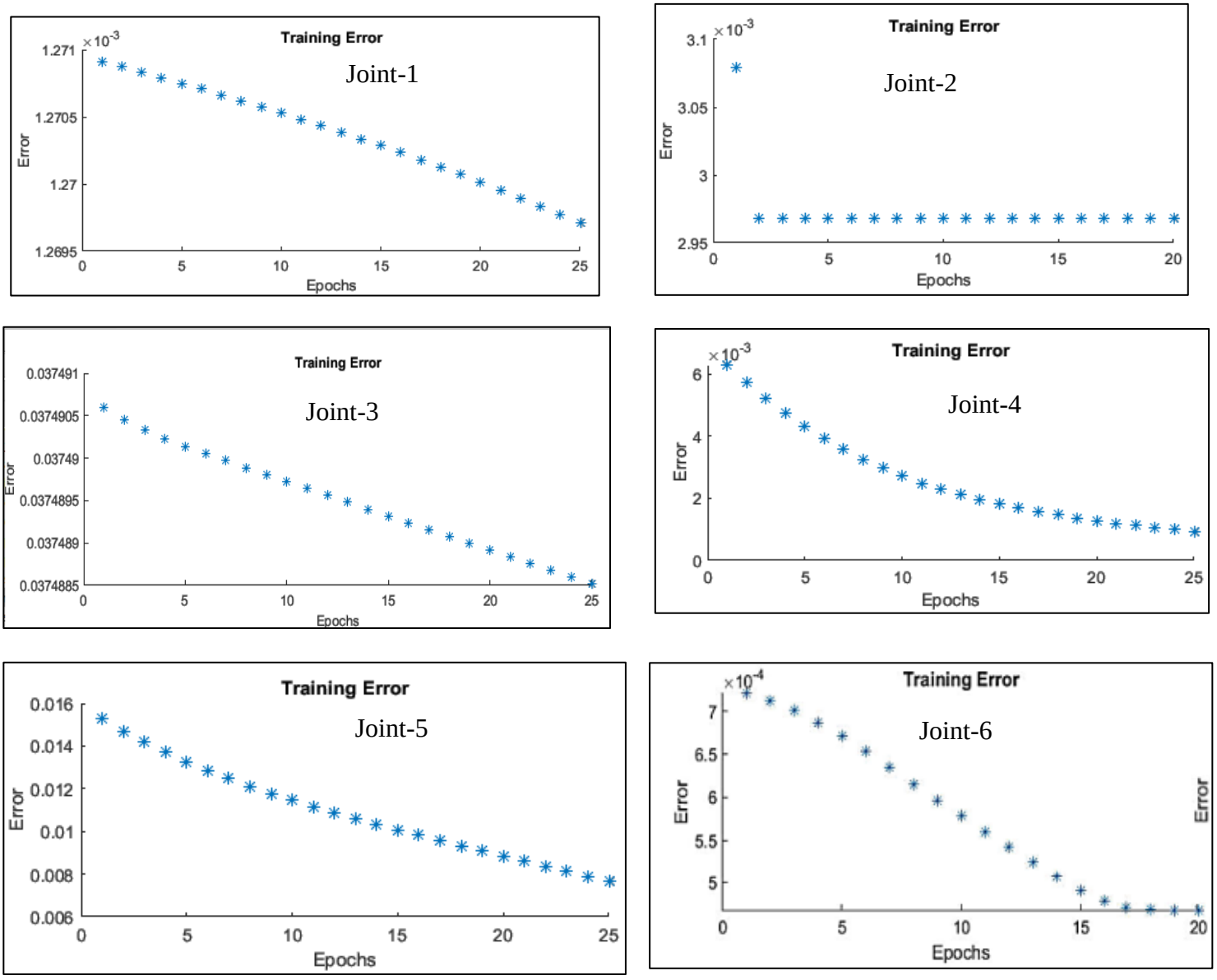

Figure 3.23: Training error of the ANFIS models

Gaussian membership functions facilitate a smooth and flexible representation of fuzzy sets, allowing the ANFIS-PID controller to effectively capture intricate data patterns while preserving the interpretability and transparency of the learned fuzzy rules. Moreover, these functions enhance computational efficiency, making the regenerative ANFIS controller ideal for dynamic control

tasks like robotic movement. Figure 3.24 presents the surface plot of the inference systems, which were derived after training the two ANFIS controllers, showcasing the models' ability to map the input-output relationships for both joints.

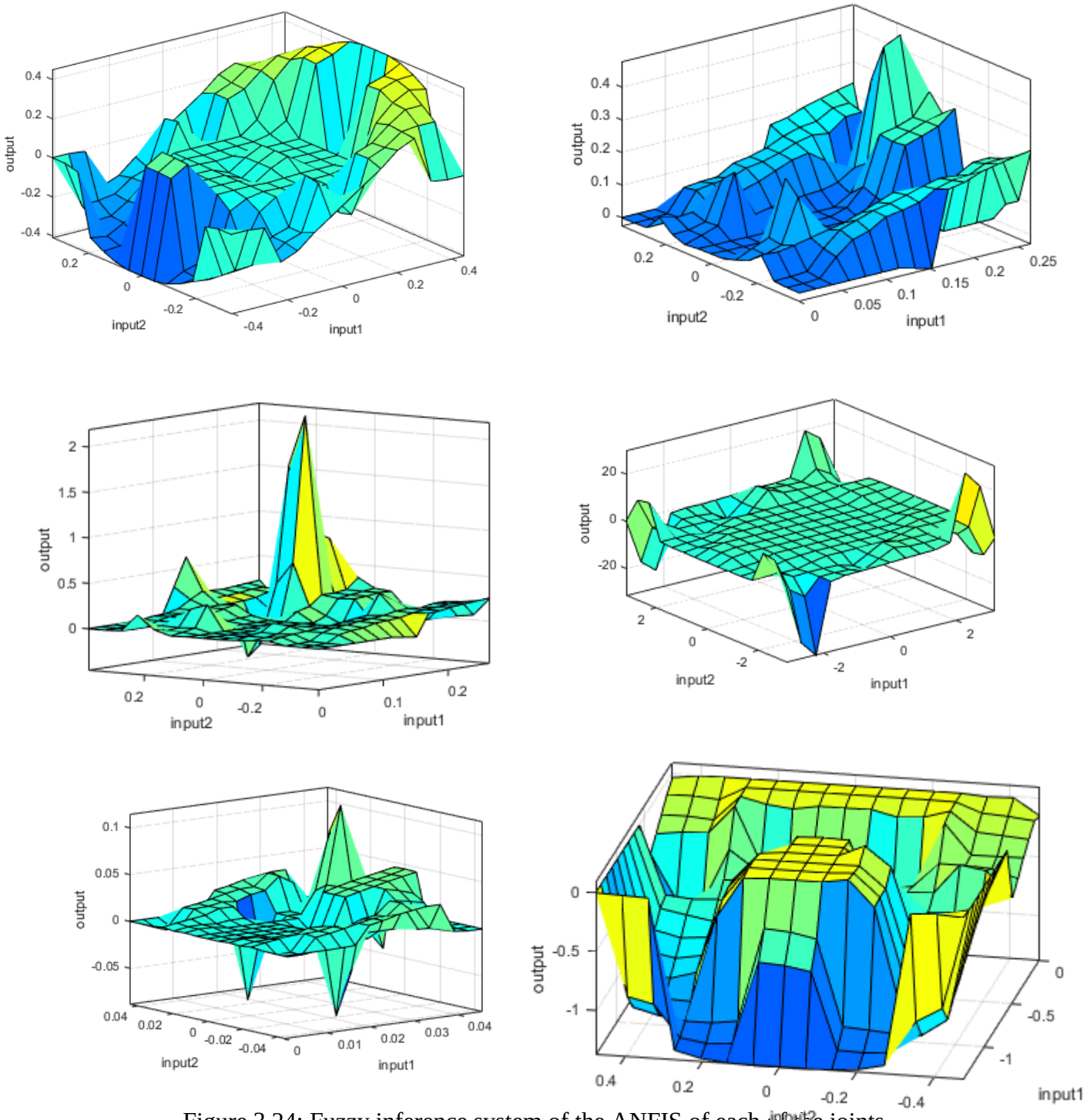

Figure 3.24: Fuzzy inference system of the ANFIS of each of the joints

CHAPTER 4

RESULT AND DISCUSSION

4.1. Validation of the Developed Inference System (ANFIS)

The ANFIS-PID controller developed for controlling the joints of the robotic system was tested and simulated under various scenarios. Given that ANFIS-PID controllers are often considered more intelligent and efficient, it was essential to compare the performance of the ANFIS-PID controller with its predecessor, the PID controller. To achieve this, a comparative study was conducted. Prior to this, the predictive capability of the ANFIS models was evaluated using the results from the PID controllers, for this purpose, a testing dataset of 13001 data points was exported from Simulink to MATLAB, based on the responses from the PID controllers. The testing was carried out using MATLAB's ANFIS toolbox, and the results are presented in Figure 4.1.

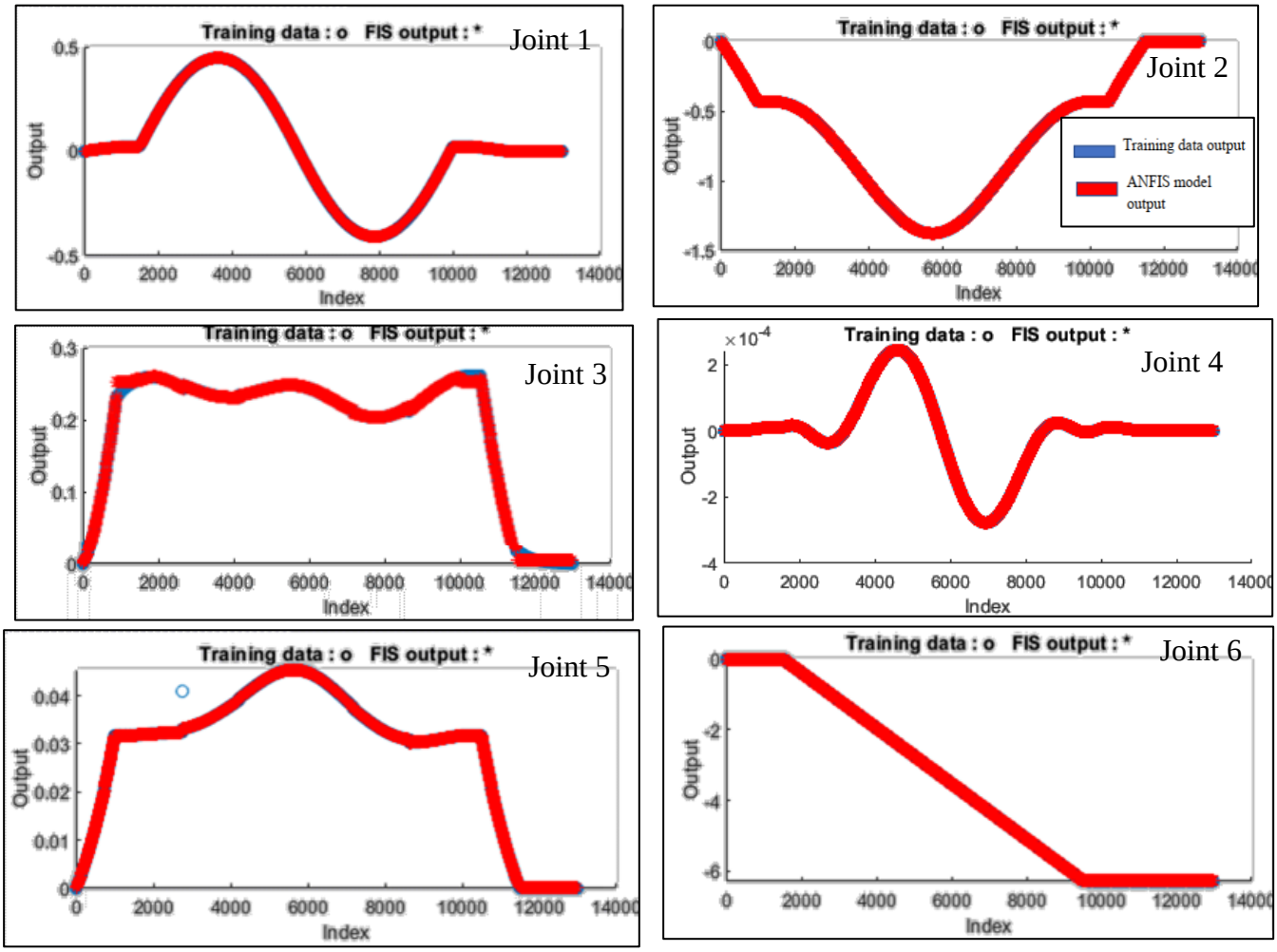

Figure 4.1: Test results of the six ANFIS models for the training data respectively

As it can be seen from **Error! Reference source not found.**, the six ANFIS models developed for e ach of the controller of each joint are predicting the output accurately with a prediction root mean squared error of 0.000127, 0.00297, 0.0037, 0.0018, 0.0077and 0.0005 respectively.

4.2. Time response analysis results of the system under no disturbance

Before subjecting the feedforward ANFIS-PID controller for the 6-DOF robot to testing under disturbances, similar to the real-world operational conditions of industrial or precision tasks, a preliminary evaluation was conducted under undisturbed scenarios. This initial phase focused on testing the controller in an ideal environment, following the designed sample trajectory designed during the development process. These undisturbed trials provided critical insights into the controller's baseline performance in achieving accurate position and orientation control, serving as a foundation for further assessments under more challenging conditions.

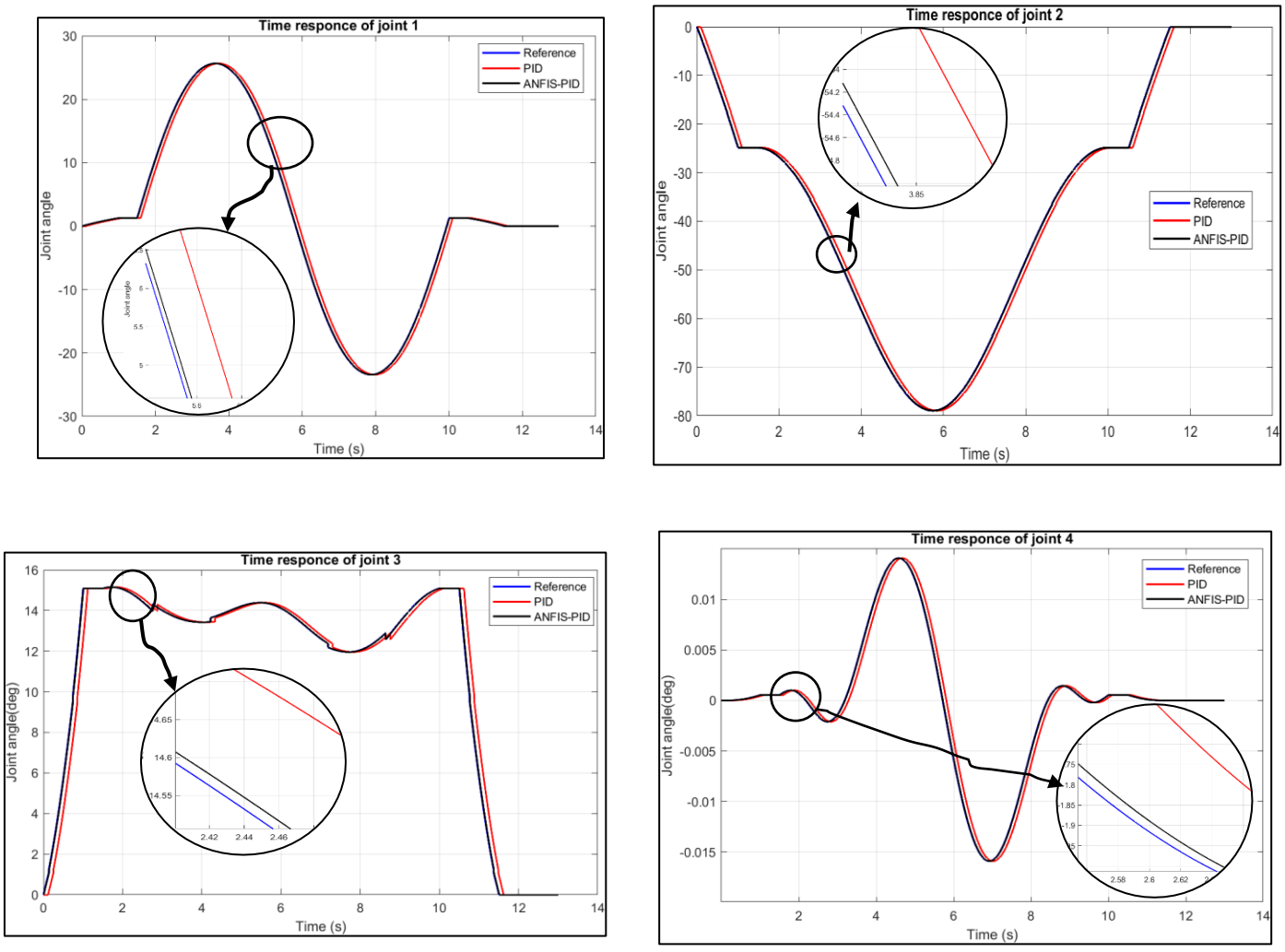

Figure 4.2: Time response of joint1 to joint 4 under no disturbance

From the time response of the 6-DOF robot's joint controllers for the reference trajectory, as shown in Figure 4.2, the PID controller exhibits varying trajectory tracking errors for each joint. For joint 1, the PID controller shows a maximum error of 2.15°, while the ANFIS-PID controller achieves a reduced maximum error of 0.12°, representing an improvement of approximately 94.41%. Similarly, for joint 2, the PID maximum error is 3.12°, whereas the ANFIS-PID maximum error is 0.23°, offering an improvement of 92.62%. For joint 3, the PID controller shows a maximum error of 1.6°, while the ANFIS-PID maximum error is 0.19°, marking an improvement of 88.12%. For joint 4, the PID controller exhibits a maximum error of 3.13°, and the ANFIS-PID error is 0.35°, reflecting an improvement of 88.81%.

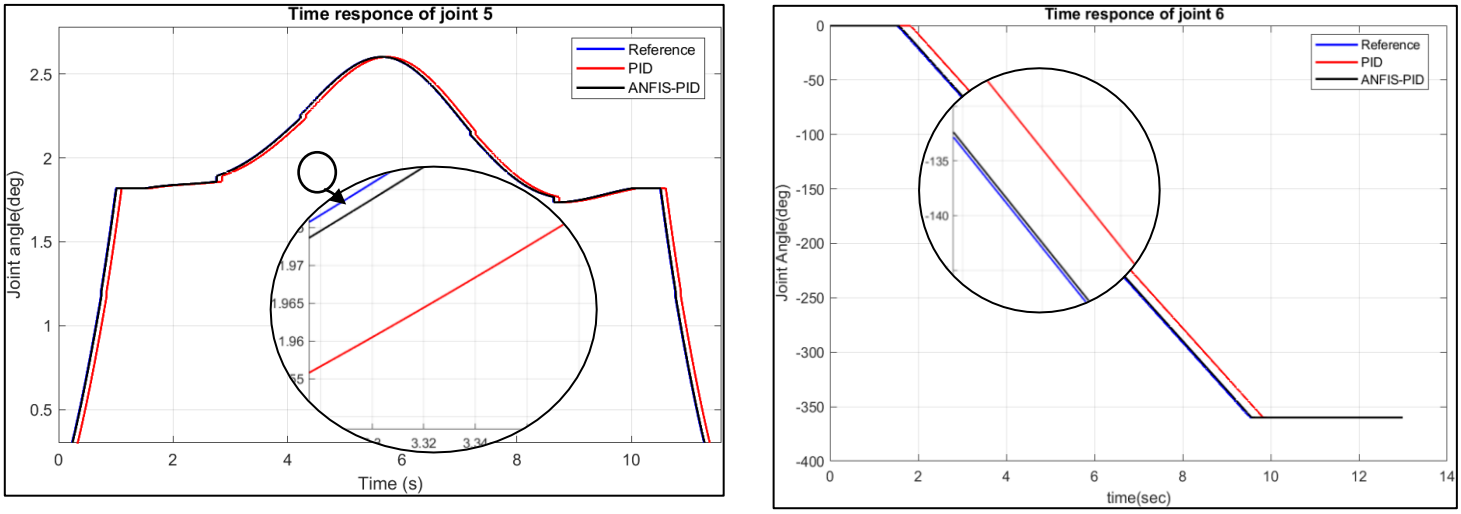

Figure 4.3: Time response of joint 5 and joint 6 under no disturbance

Similarly, for joint 5, the PID controller exhibits a trajectory tracking error of 2.11°, while the ANFIS-PID controller achieves a reduced maximum error of 0.13°, representing an improvement of approximately 93.83%. For joint 6, the PID error is 1.09°, and the ANFIS-PID error is 0.15°, marking a significant improvement of 86.23%.

In summary, for joints 1 to 6, the ANFIS-PID controller significantly outperforms the PID controller in trajectory tracking accuracy. The PID controller exhibits errors ranging from 1.09° to 3.13°, while the ANFIS-PID controller reduces these errors to values between 0.09° and 0.23°. The improvements in accuracy range from 86.23% to 94.37%, with the ANFIS-PID controller providing a substantial reduction in tracking error across all joints. These results highlight the

superior performance of the ANFIS-PID controller, ensuring precise control and making it ideal for high-quality welding tasks.

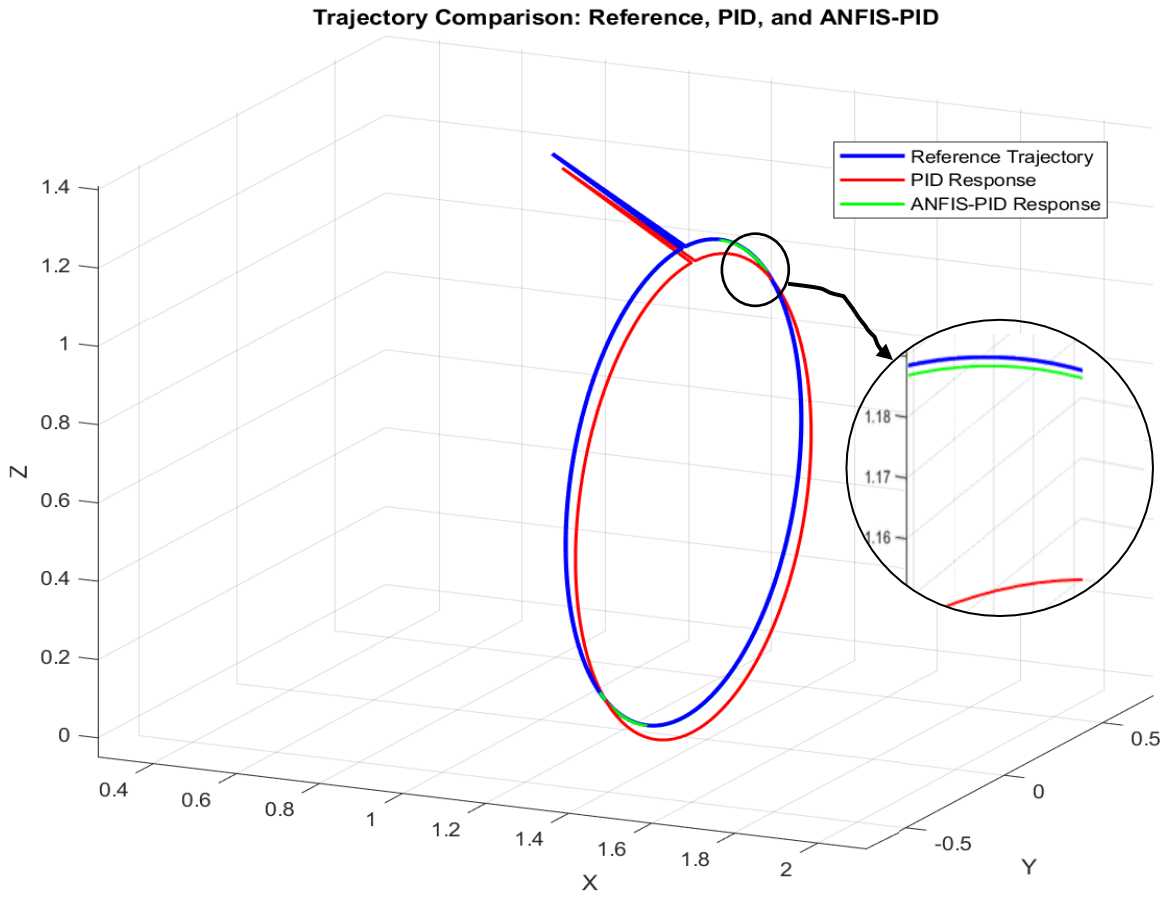

Figure 4.4: Time response of the ABB robot for the given trajectory

Using the time responses of the joint space controllers for joints 1 to 6 of the robotic arm, the trajectory tracking along the x, y, and z directions was also studied. The errors in trajectory tracking are primarily caused by the cumulative errors of each joint's space controller, with each joint's individual tracking performance contributing to the overall error in the end-effector's path. As shown in Figure 4.4, it was found that the maximum trajectory following error along the x-direction using the PID controller is 8.627 mm, while the ANFIS-PID controller reduces this error to only 1.2 mm, representing an improvement of over 86.06%. Similarly, along the y-direction, the PID controller's maximum trajectory following error is 26.825 mm, while the ANFIS-PID controller achieves only 2.56 mm, marking an improvement of approximately 90.45%. For the z-

direction, the PID controller exhibits a maximum error of 26.04 mm, while the ANFIS-PID controller reduces it to 2.5 mm, resulting in a significant improvement of 90.4%. These results highlight the superior accuracy and responsiveness of the ANFIS-PID controller in all three directions, with improvements exceeding 86.06% in each case, demonstrating its effectiveness in precise trajectory tracking for the robotic arm.

4.3. Time Response Analysis Results of The Robot Under Disturbance

Disturbances are inevitable in practical applications and can greatly influence the performance of a controller, potentially disrupting the precision and stability of robotic operations. Therefore, evaluating the controller's response to disturbances is essential for ensuring its robustness and dependability in real-world scenarios. This study incorporates the effect of external disturbances to assess the resilience of the control system, offering critical insights into its adaptive performance and reliability. To examine the behavior of the robotic arm under such conditions, a series of random noise signals with varying amplitudes were introduced, and the controllers' responses were carefully analyzed and compared.

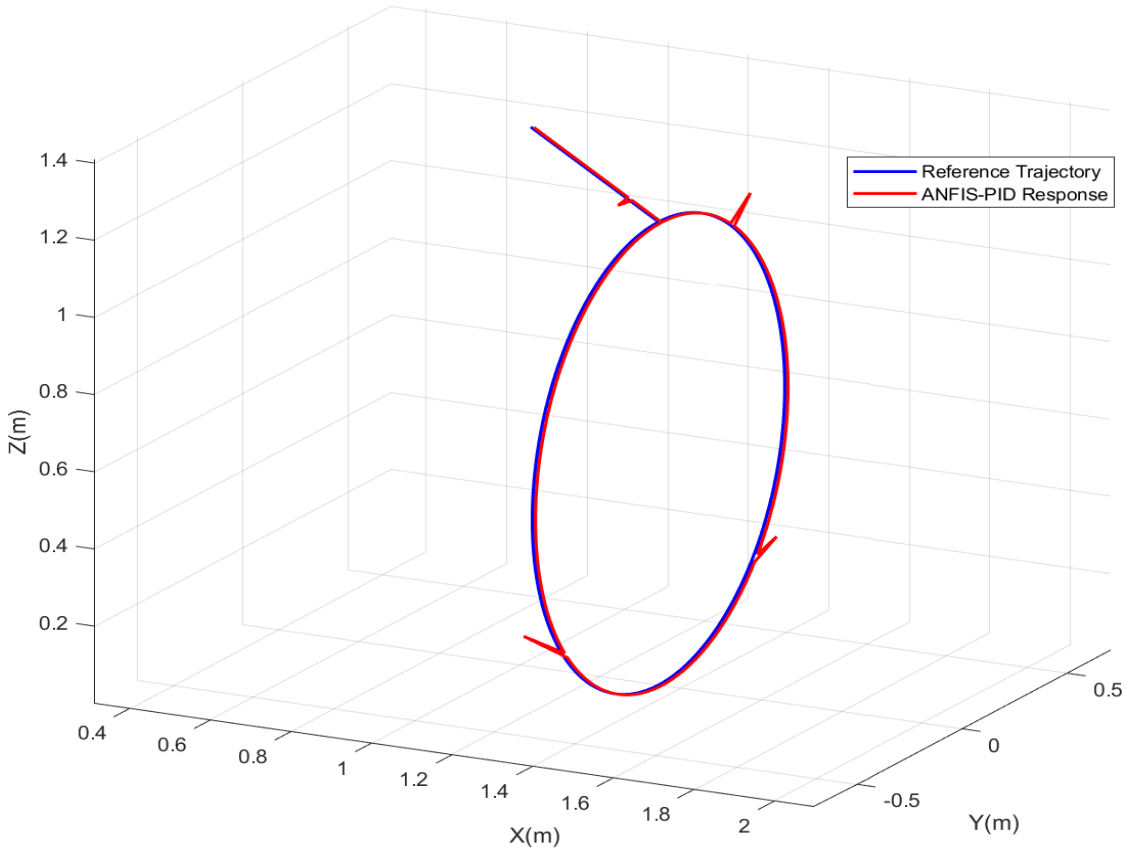

Figure 4.5: Response of the ABB robot controllers subjected to a disturbance

As seen in the time response of the two trajectories under disturbance, as shown in Figure 4.5, the ANFIS-PID controller exhibited improved robustness, maintaining a stable trajectory despite the presence of significant noise. Its adaptive nature allowed for real-time adjustments, effectively countering disturbances and ensuring a smoother path. Additionally, the ANFIS-PID controller efficiently regulated the system's behavior, minimizing deviations from the desired trajectory and enhancing the overall performance and stability of the motion, leading to a more controlled and precise operation.

CHAPTER 5
CONCLUSION AND RECOMMENDATION

5.1. Conclusion

In this research, the position and orientation control of a 6-DOF robotic manipulator was investigated through the development, modeling, and simulation of a feedforward ANFIS-PID controller. The kinematic model of the robot was constructed using the Denavit-Hartenberg (DH) convention, which facilitated the derivation of forward and inverse kinematic solutions. Verification of the kinematic model was carried out through simulations in MATLAB to ensure its reliability. A dynamic model of the robot was developed, incorporating actuator dynamics to account for the complexities of the robot's interactions. This model was constructed using MSC Adams, with SolidWorks utilized for structural modeling. The integration of MSC Adams with MATLAB/Simulink allowed for the implementation and testing of the proposed control system in a co-simulation environment. This approach enabled the evaluation of the controller's performance in a high-fidelity simulation that closely mirrored real-world conditions.

The ANFIS-PID controller was designed to improve trajectory tracking accuracy and disturbance rejection. Simulation results indicated that the controller achieved minimal trajectory tracking errors of less than 0.3° for all joints. The hybrid controller demonstrated superior performance in comparison to traditional PID controllers, particularly in handling nonlinear dynamics and external disturbances. These results confirmed the effectiveness of the proposed system in achieving precise position and orientation control. All research objectives were successfully achieved through the design and simulation processes. The findings underscore the importance of hybrid control strategies, such as the feedforward ANFIS-PID controller, in addressing the challenges of complex robotic systems.

5.2. Recommendation

Although this research achieved its stated objectives, certain limitations should be addressed in future studies. The dynamic model developed for the robot excluded the effects of link elasticity and joint friction, which are known to influence the performance of robotic systems in real-world applications. It is recommended that these factors be incorporated into future models to enhance their accuracy and reliability. Additionally, the unmodeled effects of sensor noise, thermal

variations, and mechanical wear were not considered in this study and should be investigated further to improve the system's applicability in practical environments.

The training of the ANFIS model was constrained by limited computational resources. Specifically, only 10 epochs and 10 nodes per input were utilized during the training process, which may have restricted the optimal performance of the model. The use of advanced computational systems in future work would allow for the exploration of larger datasets, more complex network architectures, and extended training iterations. These improvements could further reduce prediction errors and enhance the controller’s adaptability and precision. It is also recommended that the findings of this research be validated through experimental implementation on a physical 6-DOF robotic system. While the MATLAB/Simulink and MSC Adams co-simulation environment provided realistic testing conditions, hardware-based validation would address additional challenges, such as sensor noise, unmodeled disturbances, and hardware limitations. The outcomes of such experiments would provide a clearer understanding of the controller’s robustness and performance in practical scenarios.

Finally, the integration of other advanced control strategies, such as Model Predictive Control (MPC) or Reinforcement Learning (RL), could be explored. These methods have the potential to further optimize system performance when combined with the existing ANFIS-PID controller. By addressing these recommendations, future studies can build upon the foundation established by this research, advancing the development of control systems for complex robotic applications.

REFERENCES

[1] H. E. Jenkins, M. L. Nagurka, and T. R. Kurfess, “Robot dynamics and controls,” *Systems, Controls, Embedded Systems, Energy, and Machines*, pp. 14-13-14–37, 2017, DOI: 10.1201/9781420037043.

[2] R. N. Jazar, *Theory of Applied Robotics: Kinematics, Dynamics, and Control, Third edition*. 2022. DOI: 10.1007/978-3-030-93220-6.

[3] B. Siciliano, L. Sciavicco, L. Villani, and G. Oriolo, *Advanced Textbooks in Control and Signal Processing*. 2009.

[4] P. Sanz, *Robotics: Modeling, Planning, and Control*, vol. 16, no. 4. 2009. DOI: 10.1109/MRA.2009.934833.

[5] K. Reddy, P. Gharde, H. Tayade, M. Patil, L. S. Reddy, and D. Surya, “Advancements in Robotic Surgery: A Comprehensive Overview of Current Utilizations and Upcoming Frontiers,” *Cureus*, vol. 15, no. 12, 2023, DOI: 10.7759/cureus.50415.

[6] R. Abhishek, S. Hasa, A. Ranjan, N. Kumar, and S. Ghosh, “Research Paper on the Application of Robot Welding Technology,” vol. 10, no. 8, pp. 683–689, 2022.

[7] N. Kumar and A. Gopalswamy, “Robots in Welding of Automotive Components,” *Indian Welding Journal*, vol. 36, no. 4, p. 38, 2003, DOI: 10.22486/iwj.v36i4.178781.

[8] Jacob Rosen, Blake Hannaford, and Richard M. Satava, *Surgical Robotics*, vol. 40, no. 1. 2023.

[9] M. D. Ngo, V. H. Duy, N. T. Phuong, and S. B. Kim, “Robust control of welding robot for tracking a rectangular welding line,” *Int J Adv Robot Syst*, vol. 3, no. 3, pp. 239–248, 2006, DOI: 10.5772/5733.

[10] S. Shankar and B. Marc, “Adaptive Control Stability, Analysis.”

[11] R. Kelly, V. S. Davila, and A. Loría, *Control of Robot Manipulators in Joint Space*, 1st ed. Springer London, 2016. DOI: 10.1007/b135572.

[12] J. Denavit and R. S. Hartenberg, “A Kinematic Notation for Lower-Pair Mechanisms Based on Matrices,” *J Appl Mech*, vol. 22, no. 2, pp. 215–221, Jun. 2021, DOI: 10.1115/1.4011045.

[13] H. W. Stone, *Review of Robot Kinematics, Identification, and Control*. 1987. DOI: 10.1007/978-1-4613-1999-3_2.

[14] J. B. McConville, “Introduction to Mechanical System Simulation Using Adams,” p. 148, 2015.

[15] V. I. Utkin, “Sliding Modes in Control and Optimization,” *Sliding Modes in Control and Optimization*, 1992, DOI: 10.1007/978-3-642-84379-2.

[16] M. W. Spong, “Modeling and control of elastic joint robots,” *Journal of Dynamic Systems, Measurement and Control, Transactions of the ASME*, vol. 109, no. 4, pp. 310–319, 1987, DOI: 10.1115/1.3143860.

[17] O. Khatib, “Real-time obstacle avoidance for manipulators and mobile robots,” in *Proceedings. 1985 IEEE International Conference on Robotics and Automation*, 1985, pp. 500–505. DOI: 10.1109/ROBOT.1985.1087247.

[18] J. Y. S.Luh, M. W.Walker, and R. P. C. Paul, “On-Line Computational Scheme for Mechanical Manipulators,” *J Dyn Syst Meas Control*, vol. 102, no. 2, pp. 69–76, 1980, DOI: 10.1115/1.3149599.

[19] M. N. Bismarck-Nasr, “Nonlinear Systems,” *Structural Dynamics In Aeronautical Engineering*, pp. 119–138, 1999, DOI: 10.2514/5.9781600862458.0119.0138.

[20] R. Murray, Z. Li, and S. Sastry, *A mathematical introduction to robotic manipulation Cited by me analytic_grasp_synt... grasp_quality_metrics*, vol. 29. 1994.

[21] J. G. J. S. Vadim Utkim, “SlidingModeControlINELECTROMECHANICALSYSTEM,” 1999.

[22] W. He and Y. Dong, “Adaptive Fuzzy Neural Network Control for a Constrained Robot Using Impedance Learning,” *IEEE Trans Neural Netw Learn Syst*, vol. PP, pp. 1–13, Mar. 2017, DOI: 10.1109/TNNLS.2017.2665581.

[23] F. Merat, “Introduction to robotics: Mechanics and control,” *Robotics and Automation, IEEE Journal of*, vol. 3, p. 166, May 1987, DOI: 10.1109/JRA.1987.1087086.

[24] S. M. LaValle, “Planning algorithms,” *Planning Algorithms*, vol. 9780521862, pp. 1–826, 2006, DOI: 10.1017/CBO9780511546877.

[25] T. Mushiri and M. Moyo, “Validation of the kinematics and dynamics models of a robotic manipulator using the MATLAB robotics toolbox,” 2023, pp. 127–161. DOI: 10.1016/B978-0-323-99443-9.00008-5.

[26] S. Zimmermann, T. Berninger, J. Derkx, and D. Rixen, *Dynamic modeling of robotic manipulators for accuracy evaluation*. 2020. DOI: 10.1109/ICRA40945.2020.9197304.

[27] M. Ratiu, A. Rus, and M. Loredana Balas, “Modeling in ADAMS of a 6R industrial robot,” *MATEC Web of Conferences*, vol. 184, no. January, pp. 5–9, 2018, DOI: 10.1051/matecconf/201818402006.

[28] L. Angel, M. P. Pérez, C. Díaz-Quintero, and C. Mendoza, “ADAMS/MATLAB co-simulation: Dynamic systems analysis and control tool,” *Applied Mechanics and Materials*, vol. 232, pp. 527–531, Nov. 2012, DOI: 10.4028/www.scientific.net/AMM.232.527.

[29] Aidan. O’Dwyer, *Handbook of PI and PID controller tuning rules*. World Scientific, 2003.

[30] P. V Gopi, K. Rao, M. V Subramanyam, and K. Satyaprasad, “Model based Tuning of PID Controller,” 2013.

[31] U. M. Simulink, “Modeling and Control of Four Degrees of Freedom Surgical Robot Manipulator Modeling and Control of Four Degrees of Freedom Surgical Robot Manipulator Using MATLAB / SIMULINK,” no. November, 2015, DOI: 10.14257/ijhit.2015.8.11.05.

[32] L. Huo and L. Baron, “The joint-limits and singularity avoidance in robotic welding,” *Industrial Robot*, vol. 35, no. 5, pp. 456–464, 2008, DOI: 10.1108/01439910810893626.

[33] “Model_predictive_Controller_for_Mobile_Robot”.

[34] J.-S. R. Jang, “ANFIS: Adaptive-Network-Based Fuzzy Inference System.”

[35] N. Walia, H. Singh, and A. Sharma, “ANFIS: Adaptive Neuro-Fuzzy Inference System-A Survey,” 2015.

[36] V. Stoian and M. Ivanescu, “7 Robot Control by Fuzzy Logic.”

[37] A. A. Sadiq, G. A. Bakare, E. C. Anene, and H. B. Mamman, *A fuzzy-based speed control of DC motor using combined armature voltage and field current*, vol. 46, no. 20 PART 1. IFAC, 2013. DOI: 10.3182/20130902-3-CN-3020.00146.

[38] P. Martin Larsen, “Industrial applications of fuzzy logic control,” *Int J Man Mach Stud*, vol. 12, no. 1, pp. 3–10, 1980, DOI: 10.1016/S0020-7373(80)80050-2.

[39] K. Premkumar and B. V. Manikandan, “Stability and Performance Analysis of ANFIS Tuned PID Based Speed Controller for Brushless DC Motor,” *Curr Signal Transduct Ther*, vol. 13, no. 1, pp. 19–30, 2018, DOI: 10.2174/1574362413666180226105809.

[40] F. Liu, H. Wang, Q. Shi, H. Wang, M. Zhang, and H. Zhao, “Comparison of an ANFIS and Fuzzy PID Control Model for Performance in a Two-Axis Inertial Stabilized Platform,” *IEEE Access*, vol. 5, pp. 12951–12962, Jul. 2017, DOI: 10.1109/ACCESS.2017.2723541.

[41] M. I. Mosaad and F. Salem, “LFC based adaptive PID controller using ANN and ANFIS techniques,” *Journal of Electrical Systems and Information Technology*, vol. 1, no. 3, pp. 212–222, 2014, DOI: 10.1016/j.jesit.2014.12.004.

[42] M. H. Jali, N. E. S. Mustafa, T. A. Izzuddin, R. Ghazali, H. I. Jaafar, and My, “ANFIS-PID Controller for Arm Rehabilitation Device.”

[43] F. Liu, H. Wang, Q. Shi, H. Wang, M. Zhang, and H. Zhao, “Comparison of an ANFIS and Fuzzy PID Control Model for Performance in a Two-Axis Inertial Stabilized Platform,” *IEEE Access*, vol. 5, pp. 12951–12962, Jul. 2017, DOI: 10.1109/ACCESS.2017.2723541.

[44] M. I. AL-Saedi, H. Wu, and H. Handroos, “ANFIS and Fuzzy Tuning of PID Controller for Trajectory Tracking of a Flexible Hydraulically Driven Parallel Robot Machine,”

Journal of Automation and Control Engineering, vol. 1, no. 2, pp. 70–77, 2013, DOI: 10.12720/joace.1.2.70-77.

[45] J. Fang, G. Gu, and K.-Z. Liu, "Stability analysis for nonlinear feedback control systems with linear actuators," *Automatic Control, IEEE Transactions on*, vol. 48, pp. 649–654, May 2003, DOI: 10.1109/TAC.2003.809777.

[46] Y. Zhang and L. Jin, "Robot Manipulator Redundancy Resolution," *Robot Manipulator Redundancy Resolution*, vol. 24, no. 2002, pp. 158–168, 2017, DOI: 10.1002/9781119381440.fmatter.

[47] N. Bekiaris-Liberis and M. Krstic, "Control of Nonlinear Systems with Actuator Dynamics Governed by Quasilinear First-Order Hyperbolic PDEs," in *European Control Conference (ECC)*, 2018, pp. 1560–1565. DOI: 10.23919/ECC.2018.8550318.

[48] S. Tzafestas and G. Stavrakakis, "Model Reference Adaptive Control of Industrial Robots with Actuator Dynamics," *IFAC Proceedings Volumes*, vol. 19, no. 14, pp. 233–240, 1986, DOI: https://doi.org/10.1016/S1474-6670(17)59483-5.

[49] X. Ma, C. Wang, and J. Liu, "Adaptive control for nonlinear systems with unknown actuator dynamics based on a novel extended Nussbaum function," *International Journal of Robust and Nonlinear Control*, vol. 34, May 2024, DOI: 10.1002/rnc.7410.

[50] J.-J. E. Slotine and W. Li, "On the Adaptive Control of Robot Manipulators," *Int J Rob Res*, vol. 6, no. 3, pp. 49–59, Sep. 1987, DOI: 10.1177/027836498700600303.

[51] W. Dixon, "Control of robot manipulators in joint space, R. Kelly, V. Santibáñez and A. Loria, Springer, London, U.K., 2005, 426pp. ISBN: 1-85233-994-2," *International Journal of Robust and Nonlinear Control - INT J ROBUST NONLINEAR CONTR*, vol. 16, pp. 945–946, Dec. 2006, DOI: 10.1002/rnc.1114.

[52] M. W. Spong, S. Hutchinson, and M. Vidyasagar, "Robot modeling and control," *IEEE Control Syst*, vol. 26, no. 6, pp. 113–115, 2006, DOI: 10.1109/MCS.2006.252815.

[53] A. Robotics, "Product manual - IRB 660," 2006.

[54] R. Adebayo, C. Nwankwo, I. Festus-Ikhuoria, and O. Olajiga, "Robotics in Manufacturing: A Review of Advances in Automation and Workforce Implications," *International Journal of Advanced Multidisciplinary Research and Studies*, vol. 4, pp. 632–638, Mar. 2024, DOI: 10.62225/2583049X.2024.4.2.2549.

[55] J. Denavit and R. S. Hartenberg, "A Kinematic Notation for Lower-Pair Mechanisms Based on Matrices," *J Appl Mech*, vol. 22, no. 2, pp. 215–221, Jun. 2021, DOI: 10.1115/1.4011045.

[56] P. I. Corke, "Peter I. Corke," no. April, 2001.

[57] R. N. Jazar, *Theory of Applied Robotics: Kinematics, Dynamics, and Control, Third edition*. 2022. DOI: 10.1007/978-3-030-93220-6.

[58] M. W. Spong, “Modeling and control of elastic joint robots,” *Journal of Dynamic Systems, Measurement and Control, Transactions of the ASME*, vol. 109, no. 4, pp. 310–319, 1987, DOI: 10.1115/1.3143860.

[59] M. W. Spong, S. Hutchinson, and M. Vidyasagar, “Robot modeling and control,” *IEEE Control Syst*, vol. 26, no. 6, pp. 113–115, 2006, DOI: 10.1109/MCS.2006.252815.

[60] F. Pfeiffer, “Manipulator Trajectory Planning and Control,” *IFAC Proceedings Volumes*, vol. 19, no. 14, pp. 325–330, 1986, DOI: https://DOI.org/10.1016/S1474-6670(17)59499-9.

[61] Y. Zhang and L. Jin, “Robot Manipulator Redundancy Resolution,” *Robot Manipulator Redundancy Resolution*, vol. 24, no. 2002, pp. 158–168, 2017, DOI: 10.1002/9781119381440.fmatter.

[62] F. Pfeiffer, “Manipulator Trajectory Planning and Control,” *IFAC Proceedings Volumes*, vol. 19, no. 14, pp. 325–330, 1986, DOI: https://DOI.org/10.1016/S1474-6670(17)59499-9.

[63] A. ATA, “OPTIMAL TRAJECTORY PLANNING OF MANIPULATORS: A REVIEW,” *Journal of Engineering Science and Technology*, vol. 2, Apr. 2007.

[64] G.-Q. Sun and G.-B. Gao, “Kinematic modeling and validation of a 6-DOF industrial robot BT- Proceedings of the 2015 5th International Conference on Computer Sciences and Automation Engineering,” Atlantis Press, Feb. 2016, pp. 218–221. DOI: 10.2991/iccsae-15.2016.42.

[65] H. Nguyen *et al.*, *A review of path following control strategies for autonomous robotic vehicles: Theory, simulations, and experiments*, vol. 40. 2022. DOI: 10.1002/rob.22142.

[66] A. Robotics, “Product specification IRB 2400,” 2004.

[67] Y. H. Cho, M. S. Khan, F. Goodwin, and Y. Zhou, “Effect of torch angle and position on bead geometry and joint strength during arc brazing of thin-gauge dual-phase steel,” *The International Journal of Advanced Manufacturing Technology*, vol. 121, Jul. 2022, DOI: 10.1007/s00170-022-09309-7.

[68] D. P. Atherton and S. Majhi, “LIMITATIONS OF PID CONTROLLERS,” 1999.

[69] R. Hussain, R. Massoud, and M. Al-Mawaldi, “ANFIS-PID Control FES-Supported Sit-to-Stand in Paraplegics: (Simulation Study),” *J Biomed Sci Eng*, vol. 07, no. 04, pp. 208–217, 2014, DOI: 10.4236/jbise.2014.74024.

[70] K. M. N. C. kumar Reddy and Dr. N. Kanagasabai, “Performance Analysis of ANFIS-PID Controller based Speed Regulation and Harmonic Reduction in BLDC Motor Application,” *International Journal of Electrical and Electronics Research*, vol. 12, no. 1, pp. 187–194, Mar. 2024, DOI: 10.37391/ijeer.120127.

[71] M. I. AL-Saedi, H. Wu, and H. Handroos, “ANFIS and Fuzzy Tuning of PID Controller for Trajectory Tracking of a Flexible Hydraulically Driven Parallel Robot Machine,” *Journal of Automation and Control Engineering*, vol. 1, no. 2, pp. 70–77, 2013, DOI: 10.12720/joace.1.2.70-77.

[72] J. R. Jang, “ANFIS Adaptive-Network-based Fuzzy Inference System,” 1993, DOI: 10.1109/21.256541.

[73] J. H. Kim and S. J. Oh, “A fuzzy PID controller for nonlinear and uncertain systems,” *Soft comput*, vol. 4, no. 2, pp. 123–129, Jul. 2000, DOI: 10.1007/s005000000039.

APPENDICES

Appendix 1: Some important trigonometric identities

Pythagorean identity

$$sin^2\theta + cos^2\theta = 1$$

Angle sum and difference identities

$$\sin(\theta \pm \alpha) = sin\theta cos\alpha \pm cos\theta sin\alpha$$

$$\cos(\theta \pm \alpha) = cos\theta cos\alpha \mp sin\theta sin\alpha$$

Meaning of the function $\text{atan2}\ (y, x)$

$$atan2(y,x) = \begin{cases} sgn\ y\ tan^{-1}\left|\frac{y}{x}\right| \ if\ x > 0, y \neq 0 \\ \frac{\pi}{2} sgn\ y \ \ if\ x = 0, y \neq \\ sgn\ y\ \left(\pi - \ tan^{-1}\left|\frac{y}{x}\right|\right) \ if\ x < 0, y \neq 0 \\ \pi - \pi sgnx \quad if\ x \neq 0, y = 0 \end{cases}$$

Appendix-2: Technical data

Weight, robot

The table shows the weight of the robot.

Robot model	Weight
IRB 2600/IRB 2600 ID	280 kg

Note

The weight does not include tools and other equipment fitted on the robot.

Mounting positions

The table shows valid mounting options for the manipulator.

Mounting option	Installation angle	Note
Floor mounted	0°	
Wall mounted	90°	
Suspended	180° i	
Tilted	0-15°	Contact ABB for further information about acceptable loads.

Robot motion,

The table specifies the types and ranges of motion in every axes.

Location of motion	Type of motion	Range of movement
Axis 1	Rotation motion	±180°
Axis 2	Arm motion	+155° / -95°
Axis 3	Arm motion	+75° / -180°
Axis 4 (IRB 2600 standard)	Wrist motion	±400°
Axis 4 (IRB 2600ID)	Wrist motion	±175°
Axis 5	Bend motion	±120°
Axis 6	Turn motion	±400°

Robot dimensions

Dimensions IRB 2600-20(12)/1.65, IRB 2600 Type C-20(12)/1.65

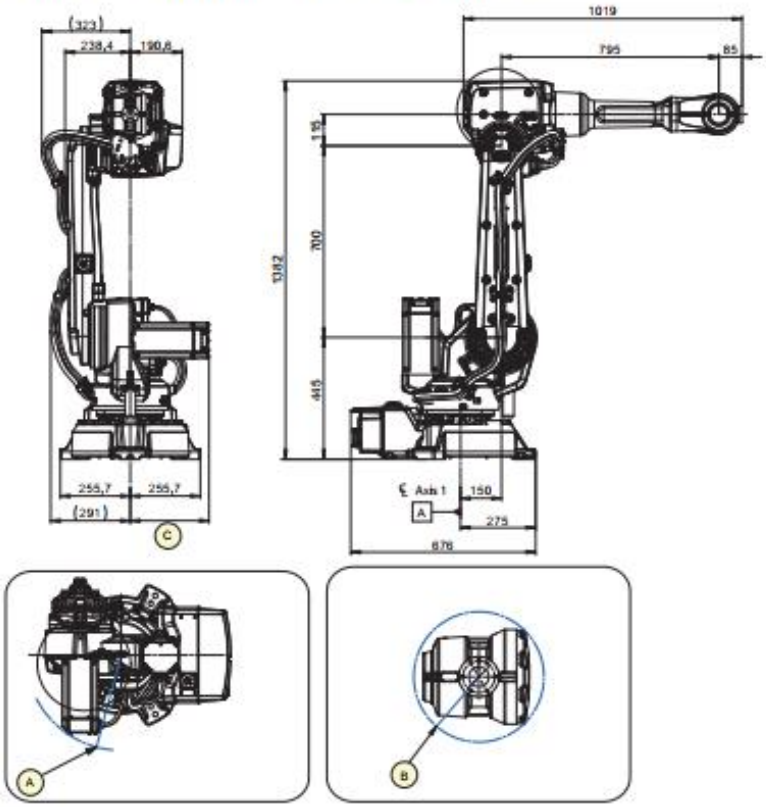

xx0900000481

Pos	Description
A	R 337 Minimum turning radius of axis 1
B	R 98 Minimum turning radius of axis 4

Turning radius

The turning radius of the robot that is floor or suspended mounted is shown in the figure.

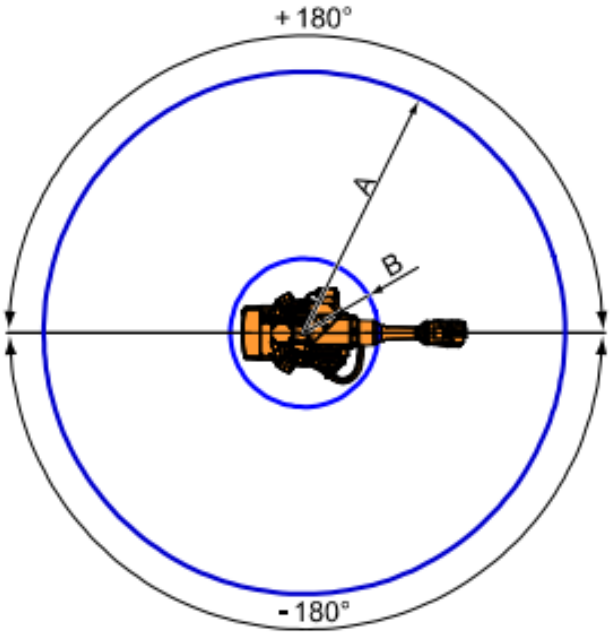

xx0900000199

Variant	Pos. A	Pos. B
IRB 2600-20/1.65 IRB 2600-12/1.65 IRB 2600 Type C-20/1.65 IRB 2600 Type C-12/1.65	R1653	R469
IRB 2600-12/1.85	R1853	R506
IRB 2600ID-15/1.85	R1850	R542
IRB 2600ID-8/2.00	R2000	R539